Faculty of Electrical Engineering
Department of Radioelectronics

Doctoral thesis

Data processing for all-sky monitoring based on Lobster-eye optics

Ing. Ondřej Nentvich

Ph.D Programme:
Electrical Engineering and Information Technology (P2612)

Specialization:
Radioelectronics (2601V010)

Supervisor:
prof. RNDr. René Hudec, CSc.

Supervisor specialist:
Ing. Ladislav Sieger, CSc.

Prague, March 2023

ABSTRACT

The Wolter type of X-ray optics is commonly used for high resolution observations, but with a narrow field of view, and therefore Wolter optics are not suitable for wide field observations. On the other hand, for all-sky or wide-field observations, a Lobster–Eye type of optics may be suitable and consists of flat mirrors that are arranged to provide a larger field of view. This type of telescope can become a promising wide-field instrument and can be used to detect interesting transient and flaring X-ray events and locate them quickly.

Part of the thesis focuses on the newly developed ray-tracing simulator PyXLA, which is mainly designed to verify the properties of the Lobster–Eye optics. It is possible to design a 1D or 2D type in Schmidt or Angel arrangement with a custom X-ray detector. Since the X-ray sky is is rich in transient, variable and flaring triggers, it is possible to include a theoretically unlimited number of sources to reflect the real situation that the instrument is supposed to observe. One of the requirements for the simulation of any X-ray optics is the implementation of reflectivity as a function of the grazing angle of incidence for the selected energy, which is also implemented in PyXLA.

In the second part of this thesis, a feasibility study is presented to locate sources from two 1D Lobster–Eye optics. This task relies on a gap created by the coded mask. The coded mask that creates the gap is in the form of a thin strip of opaque material. The proposed algorithm is mainly aimed at finding maxima and minima in the captured image. Based on the mutual position of the minima and maxima, it is possible to determine the location of the sources. For more precise localisation, images from both modules are used for cross-verification of true and false sources.

KEYWORDS

Lobster–eye optics, data–processing, simulations, X–ray, ray–tracing

ANOTACE

Rentgenová optika typu Wolter je běžně používaným typem pro pozorování ve vysokém rozlišení, ale s malým zorným polem, a proto Wolterová optika není vhodná pro širokoúhlé pozorování. Na druhou stranu, optika typu račí oko může být vhodným kandidátem pro celooblohový nebo širokoúhlý monitorovací systém, sestávající se z plochých zrcadel a jejich uspořádání je navrženo tak, aby bylo možné docílit většího zorného pole. Tento typ teleskopu se může stát vhodným zařízením ke sledování zajímavých událostí v širokém zorném poli a pro jejich rychlého lokalizování.

První část dizertační práce je zaměřena na nově vyvinutý softwarem PyXLA, který pracuje na bázi ray-tracing procesu a je zejména navržený pro ověření vlastností račí optiky. V programu je možné navrhnout jak 1D, tak i 2D typ optiky ve Schmidtově nebo Angelově uspořádání v kombinaci s rentgenovým detektorem v jejich ohnisku. Jelikož obloha skýtá plno zajímavých událostí nebo konstelací hvězd, je možné jejich rozložení nasimulovat, teoreticky až s nekonečným počtem zdrojů, aby bylo dodrženo jejich skutečné uspořádání, které se chce pozorovat. Jedním z požadavků na simulaci je implementace funkce závislosti reflektivity na limitním úhlu dopadu záření pro vybranou energii, který vyžaduje simulátor PyXLA.

Ve druhé části práce je popsána studie proveditelnosti lokalizace zdrojů záření s použitím dvou 1D optik račího oka. Tato úloha využívá mezery vytvořené kódovou maskou, která je ve tvaru tenkého proužku z rentgenově neprůsvitného materiálu. Navržený algoritmus se zejména zaobírá hledáním minim a maxim. Na základě jejich vzájemné polohy je možné určit pozici možných zdrojů zachycených oběma optikami. Pro přesnější lokalizaci je výhodné využít informaci z obou modulů pro určení skutečných a vyloučení virtuálních zdrojů záření.

KLÍČOVÁ SLOVA

Račí optika, zpracování dat, simulace, rentgenové záření, ray–tracing

ACKNOWLEDGEMENT

I would like to express thanks to my supportive family who helped me during my studies, my mentor *prof. RNDr. René Hudec, CSc.* and the supervisor specialist *Ing. Ladislav Sieger, CSc.* for many useful advices, comments and patience and also to my colleagues who support me.

Part of the thesis was prepared in cooperation with the Czech Technical University in Prague (CZE) - Institute of Experimental and Applied Physics and Faculty of Electrical Engineering, University of West Bohemia (CZE), Rigaku Innovative Technologies Europe s.r.o. (CZE), Czech Aerospace Research Centre a.s. (CZE), PANTER facility of the Max Planck Institute for Extraterrestrial Physics (DEU), Pennsylvania State University (USA), University of Colorado at Boulder (USA).

The thesis was supported by the Grant Agency of the Czech Technical University in Prague no. SGS23/186/OHK3/3T/13, SGS21/120/OHK3/2T/13, SGS18/186/OHK3/3T/13, SGS16/169/OHK3/2T/13, SGS16/150/OHK3/2T/13. The work was also supported by the EU project H2020 AHEAD2020, grant agreement 871158, and by the Grant Agency of the Czech Republic under grant no. 18-10088Y.

DECLARATION

I, Ondrej Nentvich, hereby declare that this thesis entitled "*Data processing for all-sky monitoring based on Lobster-eye optics*" is entirely my own work, unless otherwise stated. I confirm that where I have used the work of others, this has been properly attributed. Also, where part of this work is based on the work of others, I have clearly indicated this in the text.

HOW TO CITE

NENTVICH, Ondřej. *Data processing for all-sky monitoring based on Lobster-eye optics*: doctoral thesis. Prague: Czech Technical University in Prague, Faculty of Electrical Engineering, Department of Radioelectronics, 2023. 63 p. Supervised by prof. RNDr. René Hudec, CSc.

Contents

List of Figures

List of Tables

List of Codes

List of Acronyms

1D ..... one–dimensional
2D ..... two–dimensional
3D ..... three–dimensional

Athena ..... Advanced Telescope for High Energy Astrophysics

CXRO ..... The Center for X-Ray Optics

FOV ..... field of view
FWHM ..... Full Width at Half Maximum

GRB ..... gamma–ray burst
GUI ..... Graphical User Interface

HST ..... Hubble Space Telescope

IR ..... infrared
ISS ..... International Space Station

JWST ..... James Webb Space Telescope

KB ..... Kirkpatrick–Baez

LE ..... Lobster–Eye
LP ..... Long Playing

PCB ..... Printed Circuit Board
PSF ..... Point Spread Function
PyXLA ..... Python X-ray-tracing for Lobster-eye Application

REX ..... Rocket EXperiment

SPIE ..... Society of Photographic Instrumentation Engineers

UV ..... ultraviolet

WOS ..... Web of Science
WRXR ..... Water Recovery X-Ray Rocket

1 Introduction

The X-ray sky survey allows the observation of a large number of transient astrophysical sources of galactic and extragalactic origin. In the X-ray spectrum it is possible to observe various transient, flaring and persistent celestial X-ray sources, including supernovae, X-ray afterglows of gamma–ray burst (GRB) or others. To detect and observe an interesting event, wide-field telescopes/monitors are needed for fast localisation. Nowadays, satellite-based Wolter I optics are commonly used for detailed observations of astrophysical objects in the X-ray region. Their disadvantage is a narrow field of view (FOV), typically less than 1° [1]. For example, there is the Chandra orbital observatory with an 1° [2], and for the future, the large Advanced Telescope for High Energy Astrophysics (Athena) observatory is proposed, which will carry a telescope with a FOV of 0.7° [3]. Telescopes equipped with Wolter-I type optics are important for detailed analysis of distant and faint X-ray sources, but are not suitable for all-sky monitoring.

To observe a larger area of the sky, a different type of optics is required. Wide-field telescopes are able to observe a larger part of the sky to observe events simultaneously with the high-energy events. These systems are designed to detect transient objects independently and send alerts to other satellites carrying imaging optics (usually Wolter-I type), which can provide images with better spatial and time resolution of the transient or other exciting event. A suitable candidate for all-sky monitoring is a Lobster–Eye (LE) optics in a Schmidt or Angel configuration. Both types of optics can theoretically cover the entire hemisphere - up to 180° FOV [4], [5]. The Einstein probe can serve as an example of the proposed wide field LE telescopes, where its FOV is up to $60° \times 60°$ [6].

Imaging X-ray optics, e.g. Wolter types, usually work with two reflections, which leads to a greater attenuation of the incoming rays. The two–dimensional (2D) system of LE optics also has this disadvantage. This thesis proposes to split a standard LE arrangement into two 1D systems (horizontal and vertical). The output images produced by two 1D optics containing a line focus. Theoretically, a higher photon yield is achieved by eliminating losses due to double reflections, but there is only one. However, it is necessary to propose a new algorithm for image processing. The preliminary results of data processing from two 1D Lobster–Eye optics are presented in previous publications [7], [8]. We note that this approach can extend the energy range of LE telescopes to higher energies, which are otherwise limited to 8 keV or less.

Aims of the Doctoral Thesis

This thesis focuses on data processing based on LE optics, mainly for astronomical applications and use on a satellite mission. It includes a feasibility study for the detection and identification of celestial X-ray sources over a large FOV, theoretically up to 180°.

The objectives of the thesis are divided into two main topics, where the first one aims to develop a simulation program, which will be able to simulate the LE optics based on the ray tracing principle.

The second goal of the work is to develop an algorithm for source localisation using two independent 1D LE optics, which can be used as a fast monitor to determine the position of fast and interesting events in the X-ray spectrum.

Structure of the Doctoral Thesis

Chapter 2 *State of the Art* summarises information about the radiation spectrum in space and what part of the spectrum can be detected on the ground. Different principles and types of X-ray optics and their properties are also presented. Among X-ray optics, LE optics is one of the promising wide-field telescopes for locating point sources, which is the subject of this thesis.

Chapter 3 *PyXLA: Python X-ray-tracing for Lobster-eye Application* talks about the newly developed software Python X-ray-tracing for Lobster-eye Application (PyXLA), which is specifically designed to simulate the X-ray Lobster–Eye optics. PyXLA is based on the principle of ray tracing. This chapter also describes the limitations of the software and presents examples of simulations.

Chapter 4 *Point source localisation using two 1D Lobster–eye optics* introduces the localisation of sources using two 1D Lobster–Eye optics. In this chapter two principles are presented to localise the point sources. It is based on the position of the main focus and the gap created by a coded mask in the form of a thin strip of material that is impermeable to X-rays.

Chapter 5 *Conclusion of Thesis and Application* summarises the thesis and its results proposed in the objectives.

2 State of the Art

The thesis is focused on X-ray optics, specifically on the Lobster–Eye type and its data processing. The processing mainly focuses on designing the Lobster–Eye optics, processing from two 1D modules into the real image.

To introduce the problematics, we must familiarise ourselves with X-rays and X-ray optics in general and also mention the essential optics based on the reflective principle. These optics are mainly Wolter type, Lobster–Eye or Kirkpatrick–Baez (KB) type.

The following sections discuss the current state of the art, including X-ray sources and types of X-ray optics and mention several space missions that use these optics.

2.1 Space radiation

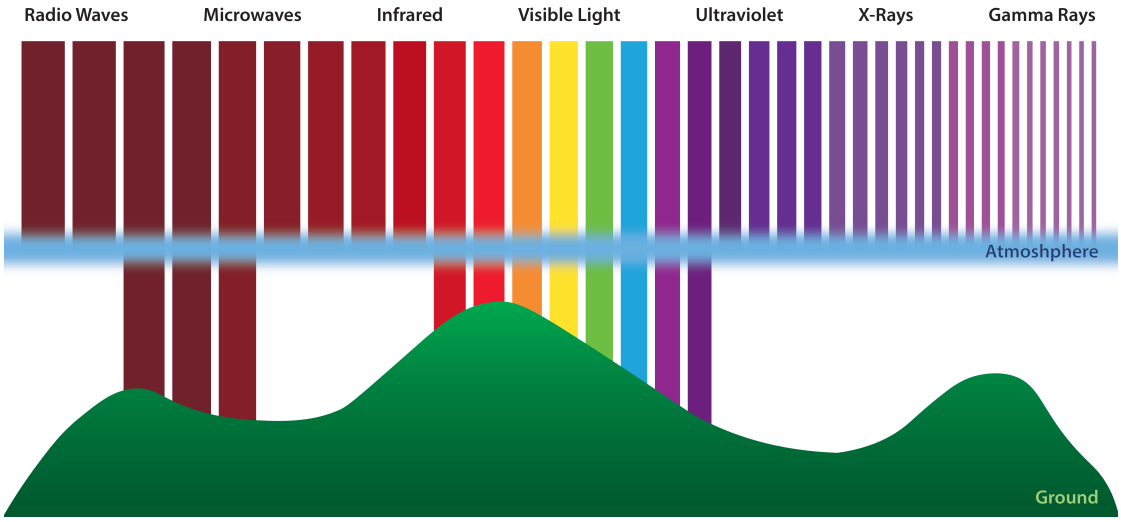

Fig. 2.1: Spectrum distribution from radio waves to gamma rays and penetration them from space to the ground with possible spectrum ranges which can be observed.

The sky appears dark in visible light because there are relatively few visible light sources in the universe compared to other types of radiation. However, in other parts of the electromagnetic spectrum, such as radio waves, infrared, ultraviolet and X-rays, the sky is filled with radiation emitted by a wide variety of celestial objects, including stars, galaxies and clusters of galaxies. Unfortunately, most of the electromagnetic

spectrum cannot be observed from the ground, as shown in Figure 2.1 and must be observed from space.

2.1.1 Infrared

A wide variety of celestial objects, including stars, galaxies, and dust clouds emit infrared radiation in space. The majority of infrared (IR) radiation is produced by warm dust and gas, often found in the interstellar medium and the spiral arms of galaxies. The radiation emitted by nearby stars heats this dust and gas, and as it heats up, it emits IR radiation. IR radiation is also emitted by cool stars, such as red dwarfs, and by brown dwarfs, which are objects that are too cool to sustain hydrogen fusion in their cores.

Infrared radiation can also study a wide range of astronomical phenomena, such as the formation and evolution of stars and galaxies, the distribution of dust and gas in the universe, and the physical conditions in distant galaxies. Because IR radiation is significantly absorbed by the Earth's atmosphere, it is better to be observed from space–based observatories such as the Hubble Space Telescope's WFC3-UVIS module [9], [10] or another famous IR mission Spitzer Space Telescope [11], [12] which was in operation for more than 16 years and was decommissioned in 2020. Last but not least mission is the James Webb Space Telescope (JWST) [13], launched in 2021, which will provide even more detailed observations of the infrared spectrum.

2.1.2 Ultraviolet

Numerous celestial objects, including stars, galaxies, and quasars, emit ultraviolet (UV) radiation in space. Most UV radiation is produced by hot, young stars [14], which are highly luminous in this part of the spectrum. These stars are often found in star–forming regions, such as in the spiral arms of galaxies. Ultraviolet radiation is also emitted by galaxies and quasars, which are powered by supermassive black holes at their centres. This radiation is produced by the intense radiation and particle winds that are generated as material falls into the black hole. UV radiation can also be scattered or emitted by gas and dust in the universe, such as in the atmospheres of planets and the interstellar medium [15].

UV radiation is also an essential tool for studying the universe. It can reveal the presence of hot gas and dust, trace the distribution of elements, and probe the physical conditions in distant galaxies. Because UV radiation is absorbed by the Earth's atmosphere, it can only be observed from space–based observatories such as the Hubble Space Telescope [9], [16], [17]. UV observations are essential to understand the formation and evolution of stars and galaxies, the distribution of heavy elements, and the interstellar medium.

2.1.3 X–rays

The last mentioned important type of space radiation are X–rays which can be divided into two kinds of origin, can be treated both as particles as well as electromagnetic waves.

X–rays as particles

X–ray particles are known as X–ray photons and can be emitted by various sources such as hot gases, stars or black holes. These X–ray photons have a very high energy and can travel through space at the speed of light. They are also affected by gravity and can be absorbed or scattered by other materials. Part of the space radiation is X–ray radiation with origin in various energetic processes in celestial objects including those related to supernovae esplosion, black holes or neutron stars.

X–rays as electromagnetic waves

X-rays can be also examined in form of electromagnetic radiation, just like visible light, radio waves, or microwaves. The main difference between X-rays and other forms of electromagnetic radiation is their wavelength. X-rays have a shorter wavelength and higher frequency than visible light, which makes them able to penetrate matter and create images of the internal structure of objects, such as various objects with different materials including human body. X-rays has usually it energy in eV units and relation between energy and wavelength is following [18]:

$$\lambda = \frac{hc}{E_\gamma} = \frac{hc}{E_{eV}E} = \frac{1.2408 \times 10^{-6}}{E_{eV}} \tag{2.1}$$

where E_γ is energy of the incoming radiation (J), h is Planc constant ($6.626 \times 10^{-34}\,\mathrm{J\,s}$), c is speed of light ($3 \times 10^{8}\,\mathrm{m\,s^{-1}}$), E is energy ($1\,\mathrm{eV} = 1.602 \times 10^{-19}\,\mathrm{J}$) and E_{eV} is energy of the photons in eV.

2.1.4 Gamma–ray bursts

GRBs are the most powerful explosions in the universe, releasing tremendous amounts of energy through gamma rays. They are thought to be caused by the collapse of massive stars or the collision of two neutron stars. GRBs are detected by satellites in Earth's orbit and can last anywhere from a few milliseconds to several minutes. GRBs typically emit gamma-ray radiation, but a large fraction of them exhibits also a X-ray afterglow emission. Depending on their duration, they can be divided into two main categories: short GRBs and long time GRBs [19].

2.2 X–ray sources

This section talks about the different X–ray sources observed in the sky where their origin can be galactic or extragalactic. The most significant X-ray binaries, various types of transients, flaring objects including X–ray sources such as gamma–ray burst, stars, supernovas, and black holes.

2.3 X–ray optics properties

The properties of the X–rays, especially for designing optics, are different if compared to visible light because they usually penetrates through the materials and is hard to focus with classical refractive lenses. Due to this fact, it is necessary to determine how to focus X–rays and study their properties, materials and parameters. Standard optics for visible light or IR use a refractive or reflective type of optics that focus rays into the focus.

Refractive optics

Due to the penetration abilities of the X–rays, it is impossible to do it this way, or the optics are too long, as is mentioned in the paper [20], where the optics has a focal length of 1.3 m and is used for high energies about 60 keV. These kinds of optics are made of tooth, and each of them is focusing the beam. It is complicated to manufacture it, but with current technologies is possible to make quite precise refractive optics for X–rays. The principle of the saw-tooth optics is depicted in Fig. 2.2. As an inexpensive X–ray refractive focusing optics can be used an old LP's as is presented in [21] which were tested at 23 keV and has quite short focus point of 22 cm. Due to the low efficiency of refractive optics, they are primarily used in laboratories for research applications.

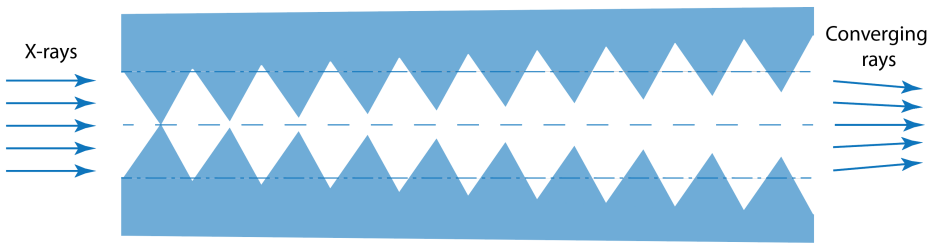

Fig. 2.2: Principle of a saw–tooth refractive optics, where incoming X–rays are on the left side, and convergent rays are on the right. The illustration is redrawn from [22].

Diffraction optics

Another type of X–ray optics is zone plate diffraction optics, often called Frenel zone planes, which work on the diffraction principle. Zone plates are made of alternating metal circular slots, which create a circular lens [23]. Zone plates are mostly used for X–ray microscopy for biology, medical or industrial X–ray imaging, e.g. Printed Circuit Board (PCB) X–ray inspection. The principle of the optical system is shown in Fig. 2.3. The space applications are very limited.

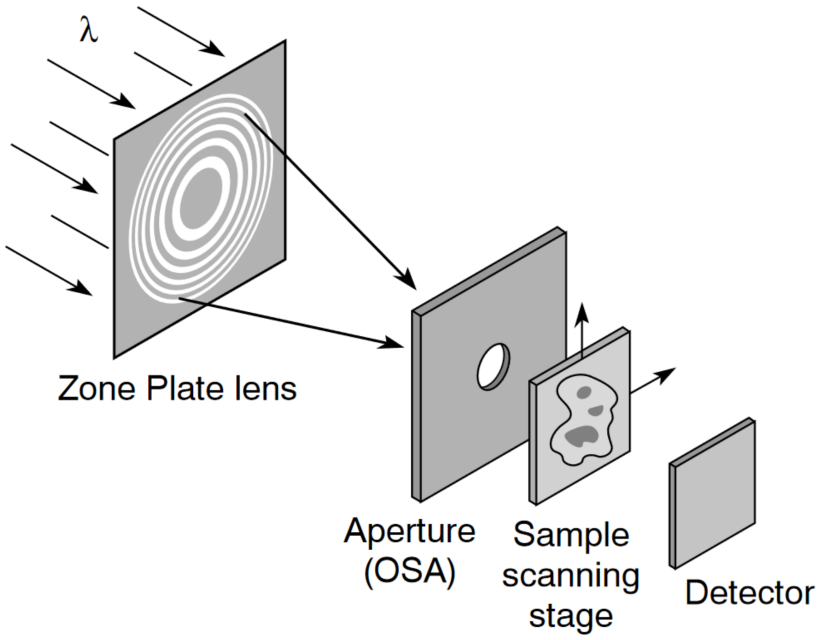

Fig. 2.3: Principle of frenel zone plane diffration optics with scanning sample and a detector [18].

Reflective optics

In addition to refractive and diffractive optics, the most useful ones are reflective types of optics for focusing X–ray radiation made by mirrors. Due to the radiation being highly penetrating through the materials, special treatment is necessary to apply for mirrors to reflect the rays. The layers mirrors are made of are usually covered with a metal layer, e.g. gold or iridium, which exhibit excellent properties for reflecting rays. Gold and iridium are also ideal for space usage because they are feasible to use under vacuum conditions and in a wide range of temperatures.

The primary and advanced types of reflective optics are Wolter-types with excellent resolution but limited FOV due to the ability to reflect X–rays. Other types can be

widefield optics LE type or Kirkpatrick–Baez (KB). Wolter type and Lobster–Eye optics are mainly used for space usage, but they can also be used for laboratory equipment including KB optics.

2.3.1 Grazing angle of incidence

Each X–ray optics is designed for limited energy spectrum, because reflectivity is very dependent on the angle of incidence. Most of the X–ray satellites have an optics designed for energies up to 12 keV, e.g. Chandra X–ray Observatory up to 10 keV [2], XMM–Newton up to 5 keV [24], eROSITA 10 keV [25] or future Athena mission up to 12 keV [3]. The reflectivity decreased for larger angles in higher energy range. In picture 2.4 there are several chosen energies and dependence of their reflectivity to the angle of incidence. Based on this knowledge, reducing the number of reflections may be preferable. The alternative can be to use an optics, which has only one reflection. 1D Lobster–Eye optics can be used for special application where high total reflectivity is required. Details about 1D LE optics are in chapter 2.6.

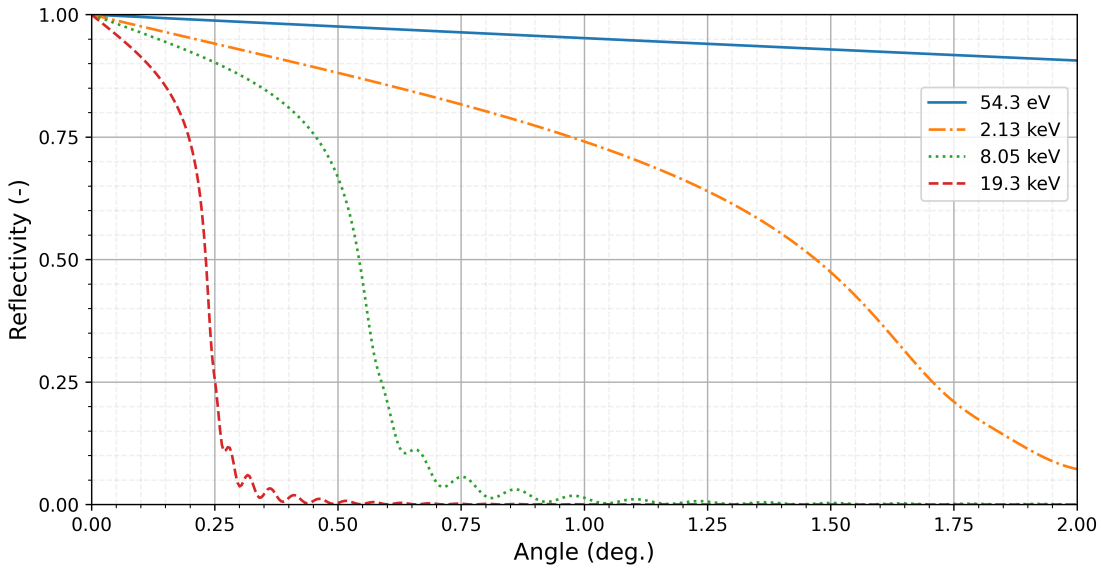

Fig. 2.4: Dependence of reflectivity on the grazing angle of incidence for energies 54.3 eV, 2.13 keV, 8.05 keV, and 19.3 keV. Data are taken from https://henke.lbl.gov [26].

Tab. 2.1: Selected elements with their emission lines [27].

Element	Energy (eV)
Li K-α	54.3
Au M-α	2 123
Cu K-α	8 048
Kr K-α	12 648
Ru K-α	19 279

2.4 X–ray optics types

One of the most popular and common reflective optics is mainly Wolter-type optics which brings high angular resolution, but low FOV, usually less than 1.0° and are used mainly for space missions, e.g. Chandra X–ray Observatory [2], XMM–Newton up to [24], eROSITA [25] or future Athena mission [3]. All of these missions use Wolter-I optics, but also exists another type of X–ray optics, particularly Lobster–Eye type, which can be wide field optics consisting of flat mirrors, which was tested, e.g. on Czech nanosatellite VZLUSAT-1 [28]–[30] or on planned Chinese mission Einstein probe with European participation [31]. The last type of X-ray optics is Kirkpatrick–Baez which has two sets of parabola mirrors while they can be made as flat mirrors and mechanically bend into the required curvature [32], [33].

2.4.1 Wolter optics

Wolter type optics consist of two types of reflecting surfaces based on the chosen type I, II or III. All types are based on hyperboloid, paraboloid or ellipsoid surface shape and their combination [1], where the first type is the type where rays hit first and then are reflected by the second type of surface. The following pictures show the principle of all three types of optics. Most optics have a symmetrical rotational shape.

- **Wolter I** consists of hyperboloid and paraboloid shape, see Fig. 2.5(a)
- **Wolter II** consists of paraboloid and hyperboloid shape, see Fig. 2.5(b)
- **Wolter III** consists of paraboloid and elipsoid shape, see Fig. 2.5(c)

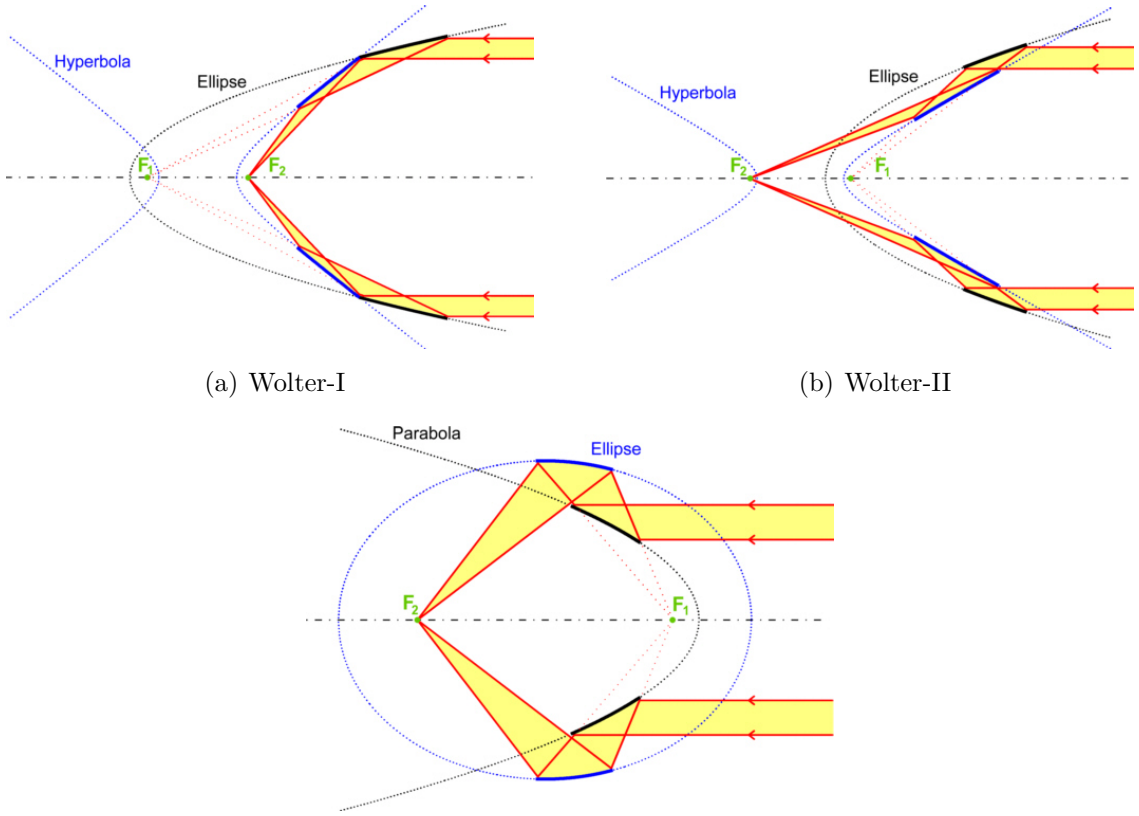

(a) Wolter-I

(b) Wolter-II

(c) Wolter-III

Fig. 2.5: Principle schematics for all three types of Wolter optics. Images are taken from [34].

2.4.2 Lobster–eye optics

The LE type of the X–ray optics is inspired by nature from an equally named animal. Their eyes are arranged to square microchannel structure, and the detailed structure is shown in picture 2.6 [33].

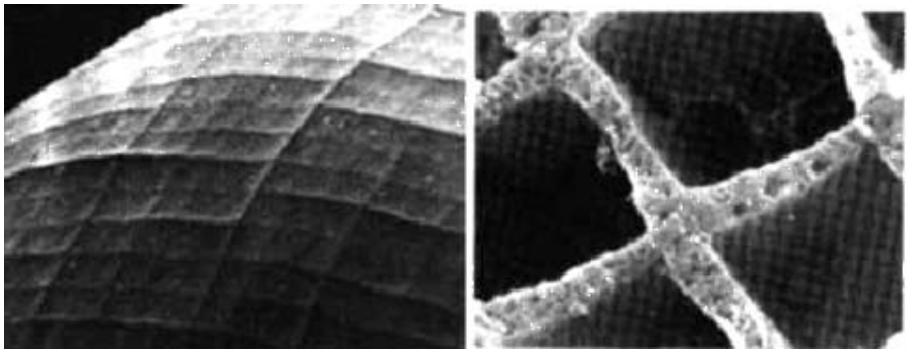

Fig. 2.6: Lobster–Eye – in the left image its surface, in the right image detailed microchannels in the eye [33]

The Lobster–Eye kind of X–ray optics exist in two basic arrangements, as is illustrated in figure 2.7. The first type is called Angel's arrangement [5] and is similar to a natural eye of a lobster. Optics in Angel's arrangement, which are artificially made, is constructed from narrow squared channels covered by a reflective material as is proposed for all-sky monitor on International Space Station (ISS) mission [35]. It is very compact, and its disadvantage is that it is hard to manufacture. It requires long and narrow tubes to produce or precise plates which are stacked together.

There is a second type called Schmidt's arrangement which has separated horizontal and vertical mirrors and is easier to manufacture because it is not necessary to make square channels, but flat or curved mirrors. It also works on double reflection principle, but the reflection from the first set of mirrors have to follow up to the second set and then to the focal point [4].

The lobster eye optics works on reflection principle and it has great potential to collect X–ray radiation in large FOV. The schematic arrangement of a lobster eye optics is in picture 2.8, where mirrors (with mirror thickness t, mirror length l and distance between mirrors a) are arranged to the cylindrical sphere side by side with radius r and with focus point F, which is equal $r/2$. This situation is better shown in picture 2.7. Incoming beam is reflected under θ angle on the surface of the mirrors to the focal point F where a detector is placed. The whole principle of a lobster eye is shown in figure 2.8 [37].

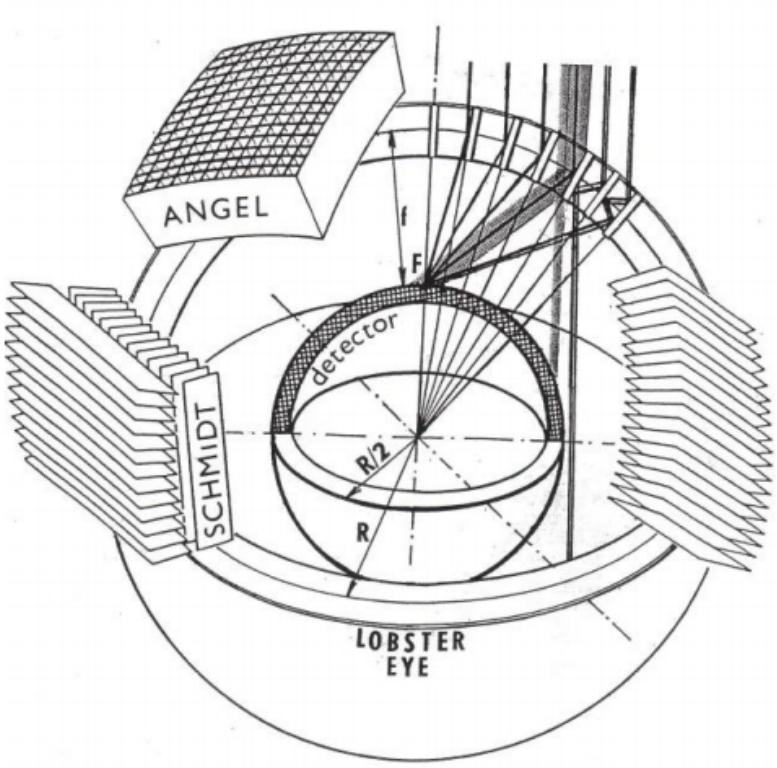

Fig. 2.7: Different arrangement of a Lobster–Eye (LE) optics in Schmidt's and Angel's arrangement [36]

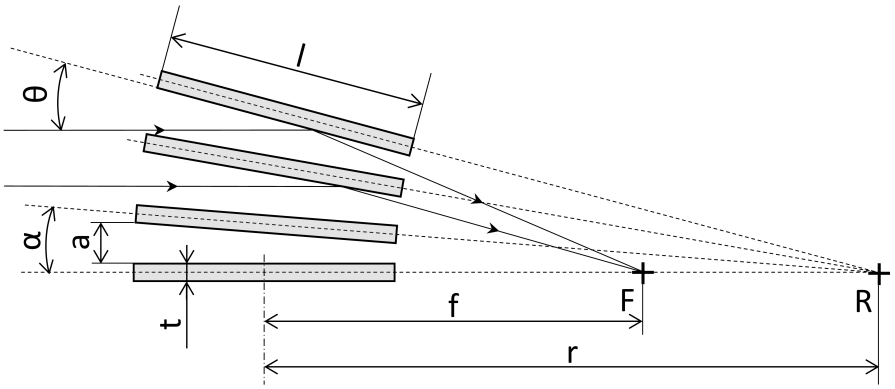

Fig. 2.8: Schematic arrangement of a LE optics with incoming rays under θ angle to the focal point F (where t is mirror thickness, F is focus point, r is radius, l is mirror length, a is spacing between mirrors, α is angle between two mirrors) [38]

2.5 Imaging 2D Lobster-eye optics

A 2D optics can create an accurate image of a subject on a detector. In case of LE types, there are Angel's and Schmidt's arrangements. These optics create a cross with a peak in its centre for a point source [4], [5]. Examples are in following pictures 2.9. In the left image 2.9, there is one point source and causes only one cross. A side-reflection causes the cross from other mirrors of the optics and by direct throughput of the beam. In case of multiple point sources in FOV, each source produces its cross as is shown in the right picture 2.9.

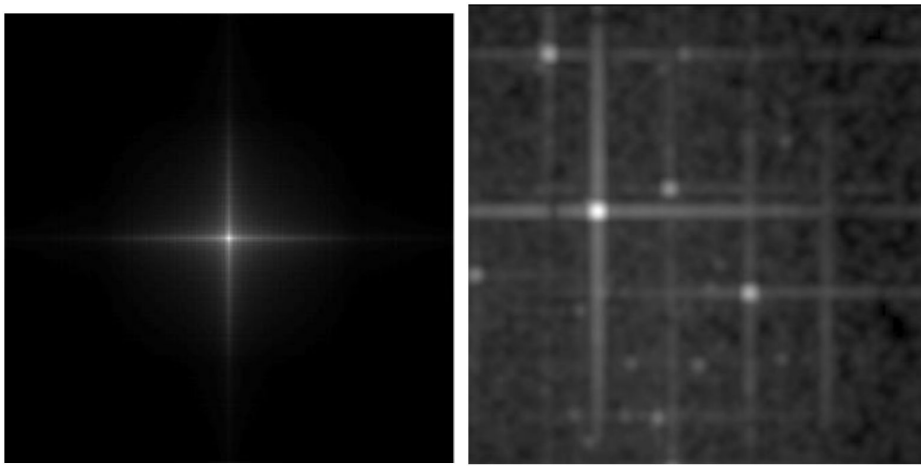

Fig. 2.9: Image produced by a Lobster-eye optics for a single point source on the left side [37] and for multipoint sources on the right side [35]

2.6 Non-imaging 1D Lobster-eye optics

1D optics is based on the Schmidt's arrangement but only with one set of mirrors, horizontal or vertical for one detector. This arrangement cannot create an accurate image like 2D system without additional improvement and post-processing. It produces only a line focus with side reflections, as shown in Figure 2.10. An advantage of using a 1D system is theoretical due to lower losses during focusing rays into the focus because they have only one reflection before beam came to the focus point as mentioned in chapter 2.3.1. Each reflection causes attenuation and is necessary to extend the acquisition time to achieve the exact count of photons. The one-dimensional system of lobster eye optics also has a higher effective aperture because the second set of mirrors does not shade it.

This system of 1D Lobster–Eye optics can be used for higher energies up to 30 keV, but for a limited field of view. The 2D system is able to work up to 10 keV with usable total reflectivity. The design of two 1D optics can be beneficial for all-sky monitoring when it is required to have an image of the sky at larger FOV [39].

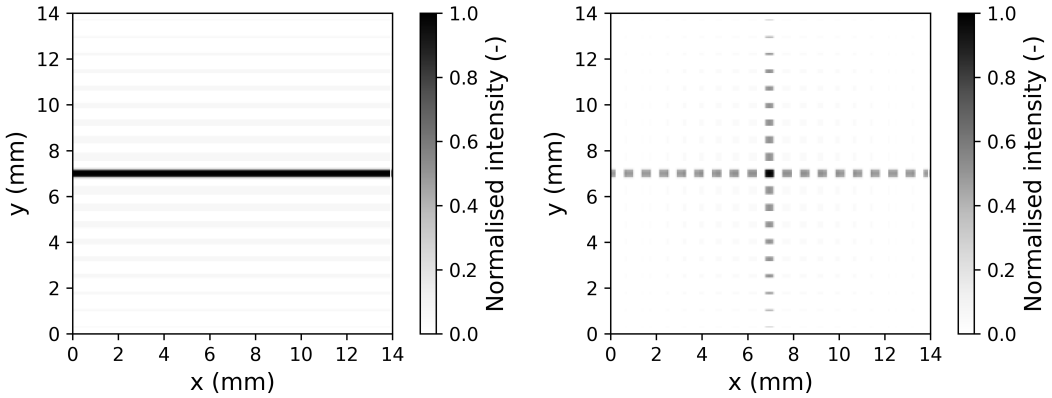

Fig. 2.10: Comparison of typical 1D (left) and 2D (right) image of a Lobster–Eye optics

2.7 Example of a Lobster-Eye optics

An demonstration of the Lobster–Eye optics is on the left side of figure 2.11. This optics was designed for the nanosatellite VZLUSAT-1 with input aperture $29 \times 19\,\mathrm{mm}^2$, focal length 250 mm and FOV 3° [28], [29]. The satellite was launched on June 23, 2017, to low orbit at an altitude of 500 km.

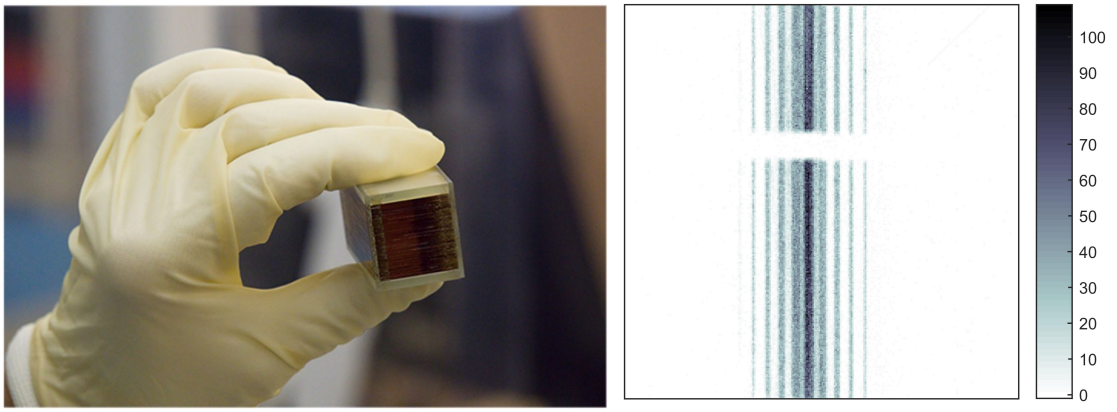

Fig. 2.11: Miniaturized LE optics for nanosatellite VZLUSAT-1 is on the left picture, and the right is an image from its testing. [28], [29]

3 PyXLA: Python X-ray-tracing for Lobster-eye Application

The Lobster–Eye optics is becoming a promising wide-field optics for observing and localising interesting events on the highly variable X-ray sky such as supernovae, GRB or others events. Due to the lack of open-source tools for simulation of the Lobster–Eye optics is available, software for simulation LE optics on a ray-tracing basis has been developed and is called PyXLA. PyXLA can be downloaded from GitLAB repository[1] and information can be found in publication [40].

This chapter describes newly developed simulation software written in Python and uses the ray-tracing principle for modelling the defined design. The PyXLA is mainly designed for the Lobster–Eye optics in X-ray spectrum and with X-ray detector, mainly from Timepix family [41] which can be thermally stabilised or not. If they are not stabilised, the measured X-ray spectrum can be distorted and needs to be compensated, as suggested in [42], [43], but the compensation is beyond the scope of this these.

The topic of this thesis is data processing with LE optics and the developed software PyXLA. The following sections describe principles, input parameters, how to work with the tool and some examples.

3.1 Input parameters

The simulation requires several essential parameters, mainly at least one source, telescope and detector, all placed in the three–dimensional (3D) space. Each component is highly configurable and can be modified in its source files when called or executed.

For all examples, following parameters listed in Table 3.1 were used.

[1] https://gitlab.com/najtvis/pyxla

Tab. 3.1: Parameters of a simulated optics which was used in the REX mission together with Timepix detector and radiation sources. Data and parameters for optics and detector were taken from [40], [41], [44], [45].

Properties	Horizontal	Vertical
Focal length	1 363 mm	1 097 mm
Foils dimensions	150 mm × 75 mm × 0.35 mm	
Number of foils in the sub–module	47	
Spacing between mirrors	0.75 mm	
Reflective surface	Au	
Reflectivity - energy efficiency	see Figure 2.4	
Detector resolution - Timepix	256 px × 256 px	
Detector pixel pitch	55 µm × 55 µm	
Radiation sources	see Table 2.1	

3.1.1 Telescope parameters

A telescope consists of one or more mirror stacks with a defined properties which are listed in the following list. An example of the creation the stack by the code is in the Code 3.1 on lines 21 and 22. There are two modules, the first with vertical stack and focal length of 1 097 mm and the second with focal length of 1 363 mm. More details about creation of the mirror stack are given in Section 3.2.2.

In the following listing there are main input parameters for mirror stacks.

- Number of mirrors
- Mirror dimension (width, height, thickness)
- Spacing between mirrors
- Radius of curvature or focal length of the module
- Reflectivity curve of mirrors for given energy
- Module spatial location
- Coatings - single or double sided

3.1.2 Detector selection

A detector is one of the simple parts of the simulation process, which can consist of only a matrix of pixels and its pixel pitch and size. Resolution or its size or shape is not limited by software, but it should be able to manufacturable to make sense for the simulation for real purpose. The resolution can range from 1 px to unlimited size and the shape can be quare or rectangular, this depend on a used type of detector. The PyXLA has now defined a set of detectors from the Timepix family [46] which can be used for simulation or can be added manually into the source code.

Summarised selected parameters which are required to define a detector are the following:

- Detector size
- Detector resolution
- Position in space
- Orientation in space

A visualisations in Figure 3.1 consists of the designed optics from previous section 3.1.1 with a Timepix detector, which was placed in the focal plane of the telescope. Another visualisation is in Figure 3.1(b) there are two optical modules with the same Timepix detector to proof that is possible to include more than one mirror stack. Visualisations were generated by PyXLA software with the enabled generation of arrangement but without plotted rays.

(a) Visualisation of an arrangement with 1D optics

(b) Visualisation of an arrangement with 2D optics

Fig. 3.1: Example of an optical system arrangement with optics and detector listed in 3.1 for two different situations where the first is with 1D and the second with 2D optics. Both cases use the Timepix detector placed in the focus of telescopes. Input aperture of the telescope is in front of the them.

3.1.3 Source of rays

A source of rays in current version[2] is modeled as an infinity source where all rays arriving at the input aperture of a telescope are parallel. Due to the fact that PyXLA is a modular system, it is possible to include another type of source which can have finite placement in the 3D space and thus the rays may not be threated as parallel. This could be used when simulation from particular point into the focus is required.
To model a source following information is required:

- Energy spectrum (a spectral line)
- Spatial position of source in 3D space
- Intensity

where the energy spectrum is especially required for properties determination of mirrors and its intensity. The rays provided by the source represent an array of rays where the intensity can be set to number 1 for obtaining an uniform telescope's Point Spread Function (PSF) or the value can be any other number or a defined array of vectors for special purposes.

3.1.4 Definition of input parameters in PyXLA

In the following Code 3.1 only elementary paramters what is necessary to set for simultaions with the particular section in the example code are chosen. Detailed input parameters are in source files with the prepared scripts *1D_lobster_eye.py*, *2D_lobster_eye.py* or in *z_axis_scan.py*. If the user can try a Graphical User Interface (GUI), in the branch of repository *gui* can be executed script *gui.py* where all input parameters are set by input boxes.

[2]In time of writing the thesis the current version was with tag v0.1

Code 3.1: Input parameters for simulations in PyXLA software with two Lobster–Eye optical 1D modules at selected energy 8.048 keV and a Timepix detector placed in the focus. Source is selected with energy 8.048 keV and matrix array of 1000×1000 rays with spacing 27.5 µm in each axis.

```
# 1.1, set detector from a list
    detectorType = 'timepix'

# 1.2, set source
    # direction of the rays
    angleX = 0.000000000
    angleY = 0.000000000

    # matrix of vector spacing and its size
    divXmm  = 0.0275
    divYmm  = 0.0275
    noPoints = (1000, 1000)

    # definition of offsets and location of focus point
    focusPoint = np.array([0.00001, 0.00001, 0.00001])
    detectorOffset = np.array([0,0,0])
    vStackOffset  = np.array([0,0,0])
    hStackOffset  = np.array([0,0,0])

# 2, create mirror modules stacks
    vStack = objects.createMirrorModule(47, 150, 75, 0.35, 0.75, True, 'V',
        focusPoint + vStackOffset, 1097*2)
    hStack = objects.createMirrorModule(47, 150, 75, 0.35, 0.75, True, 'H',
        focusPoint + vStackOffset, 1363*2)

# 5, set energies
    stp.appendEnergy(8048, "./inputs/reflectivity/8048eV.dat")
```

3.2 Principle

A general scenario of any reflective optics is based on the reflection principle described in the theoretical part in section 2.3.1 together with a grazing angle of incidence which is essential for X-ray optics. The principle of simulations has been already introduced in [47]–[49] and these all models were on analytical basis. The code in PyXLA can be divided into several factors: reflectivity, mirror creation and ray-tracing.

3.2.1 Reflectivity

As mentioned in section 2.3, every X-ray optics has its limiting angle where it can be operated. It is caused mainly by decreasing reflectivity with angle and energy according to Figure 2.4. These curves are for specific materials, coatings and compositions, but generally, with greater angles, reflectivity decreases. This dependency is mandatory to implement into the ray-tracing, otherwise, the result will be calculated with constant reflectivity, e.g. 100 %. The reflectivity of 100 % or nearly to 100 % can be helpful for using visible light, but with X-rays not, it will not reflect the real situation. A comparison of different reflectivities for LE optics is in Figure 3.2. The reflectivity is represented by the percent value for mirrors without losses, and variable value depends on energy according to Figure 2.4.

The source in the Figure 3.2 is shifted by 0.2° as an apparent influence of the incoming energy. In Figure 3.2(b) is clearly visible detail that at energy 19.2 keV is difficult to reflect rays, and the second peak at 12.2 mm is attenuated. This is caused by the fact that at 0.3° the reflectivity for 19.2 keV is only about 5 %, but at 0.2° it is still around 70 %. But for energy 2.13 keV the reflectivity is about 95 % for both angles and thus the second peak is present.

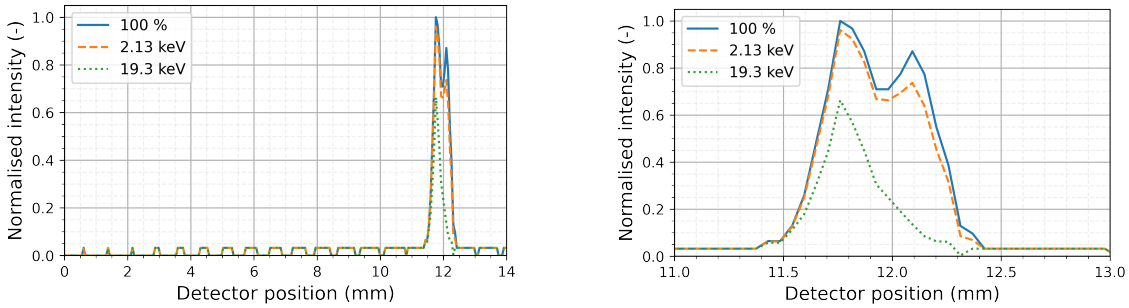

(a) complete cross-section

(b) detail of the cross-section 3.2(a) in the range from 11 to 13 mm

Fig. 3.2: Comparison of different reflectivities, where solid blue line is for 100 % reflectivity, dashed orange is for 2.13 keV and dotted green is for 19.2 keV. Source was placed off-axis by 0.2° which created a peak around 11.8 mm. Images are taken from [40].

The reflectivity for each energy is stored in a separate file. It contains angle, reflectivity and transmission into the substrate as was obtained from online source The Center for X-Ray Optics (CXRO)[3]. Updating a file into the specific format as is in the following listing 3.2 is required.

[3]https://cxro.lbl.gov/

Code 3.2: Input file with reflectivity data, particularly for 2.13 keV. Only the beginning of the file is shown.

```
Au 30.nm on SiO2 at 2123.eV, P=0.
Angle (deg),Reflectivity,Transmission into substrate
0.000000,1.00000,0.000000
1.002004E-02,0.997580,1.079265E-11
2.004008E-02,0.995165,2.158829E-11
3.006012E-02,0.992755,3.241611E-11
...
4.97996,1.610782E-03,0.506146
4.98998,1.640288E-03,0.506893
5.00000,1.660578E-03,0.507641
```

PyXLA's raytracing process uses this data file as a lookup table for specific angles for each ray. The closer lower angle is used if the incoming rays differ from the angle in the data file. If the lookup table is limited, e.g. to 5°, because there is no useful reflectivity data above that angle, in this case all angles above 5° are treated as the largest angle in the dataset, the last row of the lookup table.

3.2.2 Mirror stack creation

One of the most important part in the simulation is definition of each mirror, its properties and position in the mirror stack of the telescope. Arrangement of the mirrors and stack itself depends mostly on the target application, mainly on energy range and detection FOV. Due to the fact that the Lobster–Eye can be a wide-field optical system, the mirrors are generated uniformly on the perimeter of radius of curvature which creates an arc from the mirrors as is illustrated in Figure 3.3. The distances between mirrors are determined in their geometrical centre with their spacing a as described in Figure 2.8.

In the basic approach as defined in the previous chapter 2.4.2 in schematic Figure 2.8, due to the fact that the Lobster–Eye optics represent wide-field optics, all mirrors in the stack are uniformly and symmetrically spread out from the optical centre in a defined spacing a (measured in the geometrical centre of mirrors). The angle α is related to the radius of curvature $\mathbf{R}$ and is the angle between two neighbouring mirrors. The angle α should not exceed the critical angle where the reflective layers don't reflects rays or with low efficiency well, e.g. for Au M-α spectral line at 2.13 keV is critical angle about 1.6° for a golden layer according to Equation 3.1 [18]. The reflectivity is energy-dependent and related to Figure 2.4.

$$\theta_c = \sqrt{2\delta} = \sqrt{\frac{n_a r_e \lambda^2 f_1^0(\lambda)}{\pi}} \tag{3.1}$$

Due to the fact incoming rays can be captured from different directions (in terms of FOV of the optics) and only several mirrors can catch them, it is viable to use double-sided mirrors to extend FOV. The simulation can be used or not and depends on the target application.

When the module stack is created, the next step is to place it in the proper position in the 3D space, which should be in the focal length of the designed optics from the detector. An example of a created optical stack is in the following Figure 3.3 with 47 mirrors.

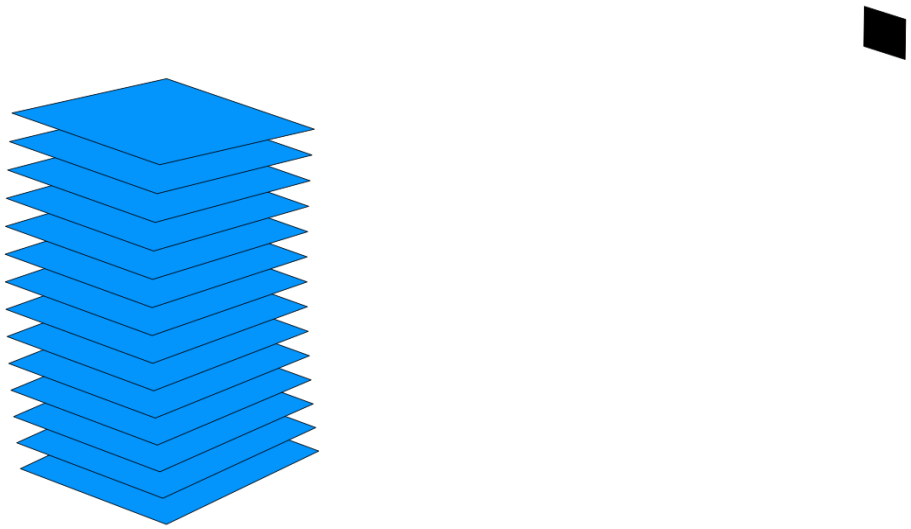

Fig. 3.3: A detailed example of a general mirror stack (left blue stack) designed by PyXLA software with 14 mirrors and a detector on the right side

3.2.3 Ray-tracing

As was mentioned before, the core of the PyXLA software is based on the ray-tracing process, which is responsible for creating an X-ray image on the detector. This step supposes to be already defined the detector and mirror stack. The last step is to create a source which executes the ray-tracing process. The process is made for each source and consists of several steps, which were introduced in [40] and are the followings:

1. Define an 2D array of rays and spacing between them
2. Select the initial intensity of rays from the predefined set of types (uniform, random, custom)
3. Set the position of the array of rays in the X and Y axis (elevation and azimuth)
4. Execute the ray-tracing process by sending each ray from the array toward the input aperture
5. If each ray hits the mirror, its intensity is proportionally decreased according to the energy and grazing angle of incidence (see Figure 2.4 and section 3.2.1)
6. Due to the ray-tracing process can be time-demanding, parallel processing is applied when the number of rays exceeds 1 000 rays per core
7. When the ray hits the detector, the affected pixel increases its own intensity of the ray's remaining intensity. If the ray misses the detector, it is discarded, and the next ray is performed
8. After execution of all rays, each pixel of the detector's matrix includes the total accumulated intensity

When all sources are executed, the ray-tracing process finish. The results are then stored in the 2D matrix in the detector, which can be stored as a file or visualised as an image. Several examples of the images are in the following section 3.4.

A visualisation of the setup, including rays with their origin in infinity are depicted in the following Figures 3.4, where the first one 3.4(a) is with a source placed on the optical axis and the second in 3.4(b) was declined by 0.7° off-axis. The colours of the rays are the following: red are direct rays, orange are once reflected, and green rays are reflected more than once.

For the source placed on the optical axis, the rays are reflected to the centre of the detector and it is in agreement with the theoretical prediction. In the second case with a source declined by 0.7° the rays coming from bottom and are also reflected to the bottom part of the detector. Based on the results where the mirrors stack has focal lenth of 250 mm and length of mirrors is 75 mm, this angle is limit for this particular setup. This arrangement was seleced regarding mainly for visualisation of the behaviour.

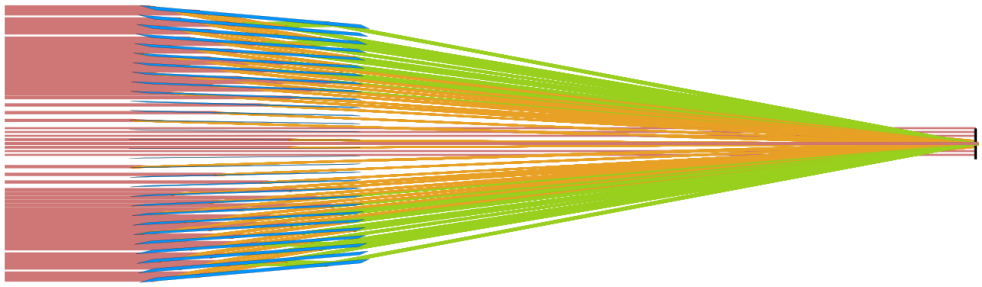

(a) Visualisation of an arrangement with a source placed on the optical axis

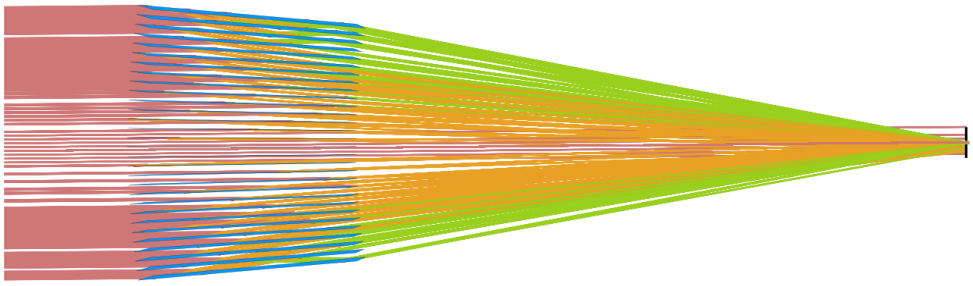

(b) Visualisation of an arrangement with a source placed 0.7° off optical axis

Fig. 3.4: Simulated 1D optics and Timepix detector with one source placed in infinity and parallel rays from its origin. The design was adjusted regarding for visualisation.

3.3 User interface

The PyXLA is written in Python, a scripting language, and the processing can be customised according to target demands, as are examples in the repository. On the contrary, developing a GUI, also part of this software, is highly recommended for the user-focus application. It consists of elementary parts such as the definition of the optics, detector and radiation sources. In the following Figure 3.5, there is one of the first approaches of the GUI. It is separated into specific parts, as was mentioned.

The current version of GUI cannot change the stack's offset, and this can cause the double maxima in focus. As well as, there is a lack of defined mirror stacks which can be beneficial for the review of the defined optical elements. In the summarised image of the output in Figure 3.5, two cross-sections are taken in the middle of the resulting image. They serve mainly for the initial verification of the PSF and target gain as well.

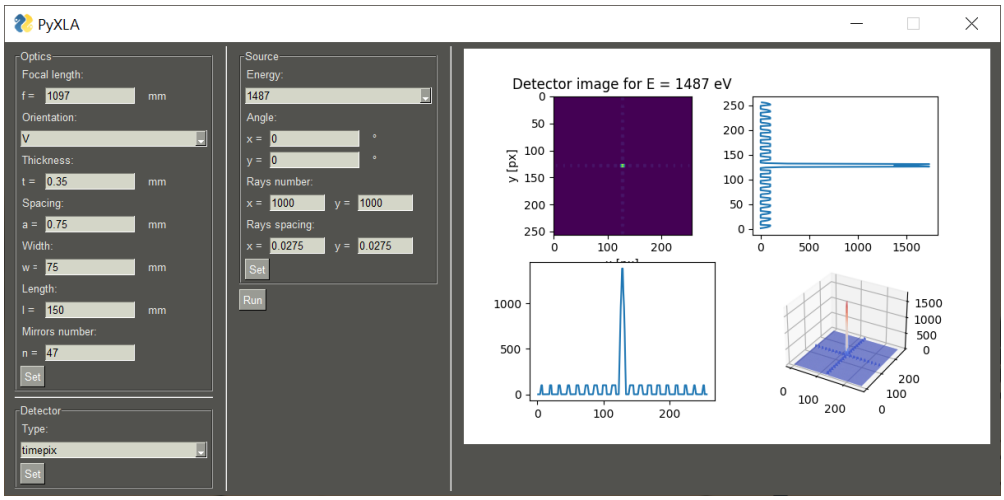

Fig. 3.5: GUI of the PyXLA software with 2D optics in angel's arrangement, with the focal length of 1 097 mm

3.4 Potential application of the simulator

Our team has recently participated in several Lobster–Eye missions, namely VZLUSAT-1 in collaboration with Aerospace Research Centre, carrying a 1D Lobster–Eye telescope with Timepix detector [28], [29], [50]. Or it participated in another Water Recovery X-Ray Rocket (WRXR) mission called Rocket EXperiment (REX), which carried two LE telescopes, the first of 1D type with the same characteristics as in the previous mission of VZLUSAT-1 and the second telescope with the 2D Lobster–Eye optics [45], [51], [52]. The REX mission was set up in collaboration with the University of Pennsylvania, which provided space for this experiment. Because of the two LE telescopes, no detailed study has been done and it is based on this fact that the development of the PyXLA simulator was started.

In this thesis I have tried to verify the properties of the LE telescope from the nanosatellite VZLUSAT-1 and the same optics from REX and compare them with the simulations. Based on the comparison shown in Figure 3.6, it can be verified that the focal length given in [45] is higher than the results from the simulations. Also the position of the examined optics is shifted by 20 mm, which was shifted as well as in the simulator.

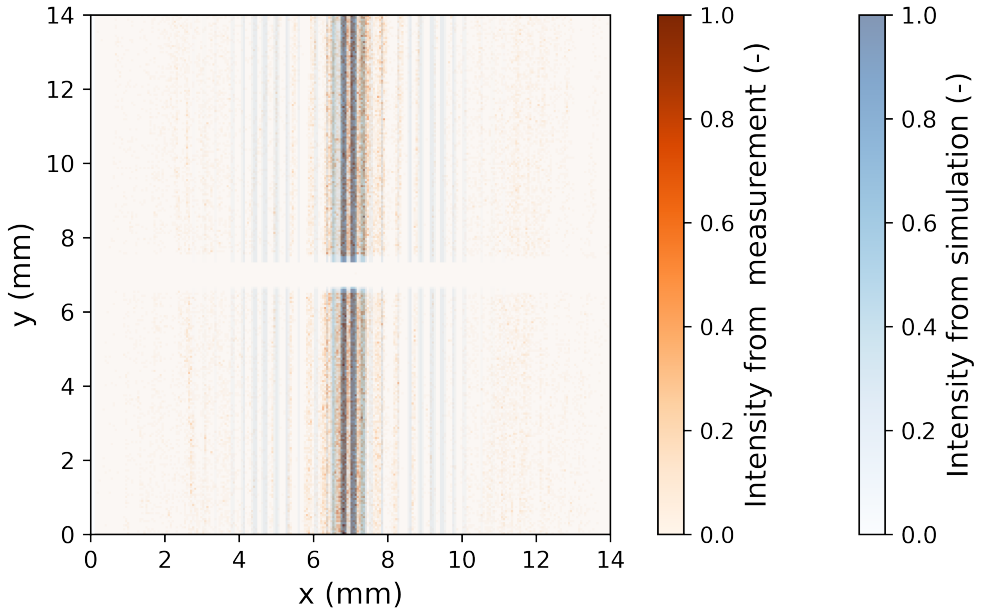

(a) Image from the detector from measurement and simulations

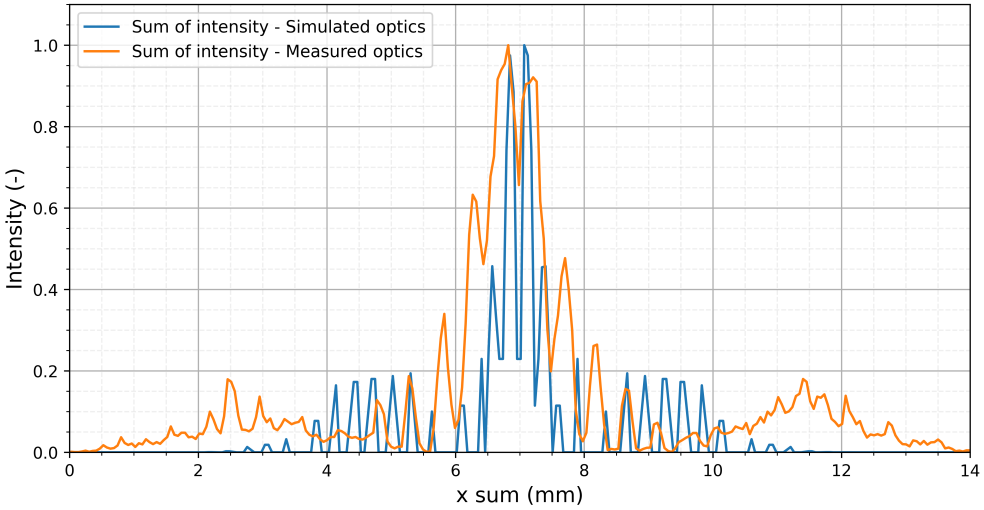

(b) Sum of rows from the measurement and simulations

Fig. 3.6: Comparison of the Lobster–Eye optics from VZLUSAT-1 mission with focal length of 243 mm and theoretical results given by PyXLA simulator with shifted detector by 20 mm. The measurement and simulation was performed with radiation source of 8.05 keV.

4 Point source localisation using two 1D Lobster–eye optics

Astronomical X-ray sky is full of interesting transients or phenomena, which are usually very weak and catching every photon is valuable to achieve information about position of each source. Due to the fact that the One–dimensional Lobster–Eye optics can work as a collimator or a concentrator with only one set of reflective mirrors (compared to a Wolter or 2D Lobster–Eye optics), theoretically is possible to reach better results with higher photon yield. The photon yield for the same grazing angle of incidence can be better where the reflectivity factor, as was introduced in section 2.3.1. This claim is useful for the grazing angle of incidence, which is useful, e.g. for 8.05 keV can be 0.65°. Based on this idea it can be achieved higher photon counts reached the detector and thus decreased capturing time for the same bright/weak observed objects. The 1D Lobster–Eye optcis can have one disadvantage that the detector should be long to acquire complete focus line produced by the source; acquire as much photons as possible for the source.

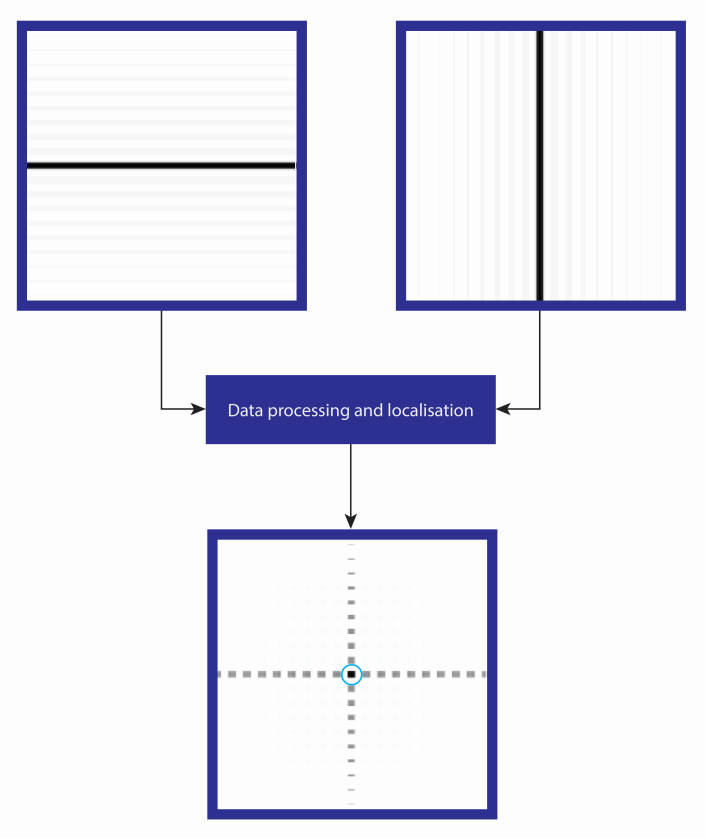

Fig. 4.1: Idea of data processing from two 1D Lobster–Eye optics.

The idea of the processing is illustrated in Figure 4.1, which requires two independent 1D images to be captured simultaneously. This solution has a disadvantage because it requires two optics, ideally rotated by 90° and two detectors which will collect focused incoming photon flux. These detectors consume additional power in case the condition of simultaneous image capturing. Power demands are crucial especially for space usage where the power is limited as well as weight, but for the laboratory usage, it should not be critical. The principle of the design is illustrated in the following image Figure 4.2. The source code for the processing can be downloaded from GitLAB repository[1].

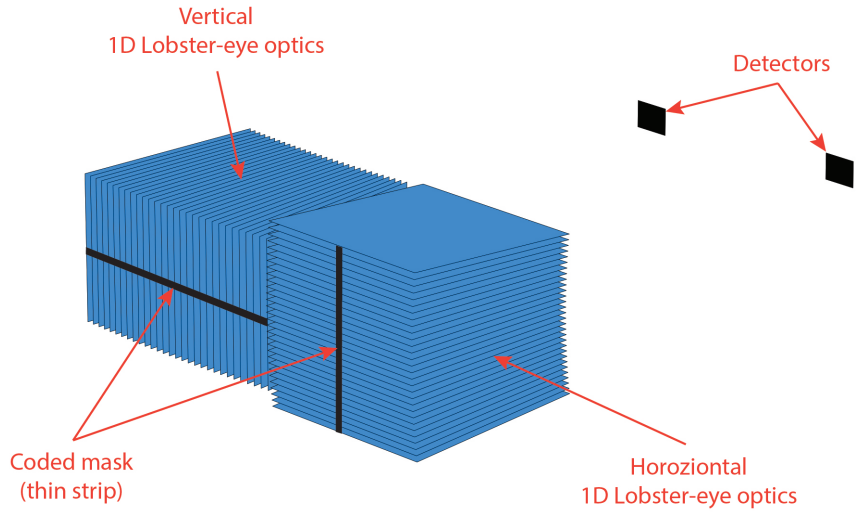

Fig. 4.2: Two independent 1D Lobster–Eye optics with their own coded mask as a thin strip placed in front of each optics [38].

Since both detectors and optics are independent as shown in Figure 4.2, there is no strict reason why both optics should have the same parameters such as focal lengths, number of mirrors or any other parameter. If they have the same parameters, there is no further processing because they have the same FOV. But if it is necessary to have different parameters, e.g. due to construction or other reasons, it is necessary to compensate some properties such as FOV. This is demanding for the correct next post-processing.

Image captured by a 1D Lobster–Eye optics produces a line focus with side reflections or direct light. This is caused because the perpendicular optics module is also missing from Schmidt's arrangement and, thus, the second reflection into the focus. The information obtained from the 1D image is only one direction of the incoming rays. Suppose the second 1D optics with the second detector is placed in the system

[1]https://gitlab.com/najtvis/localisation-using-two-1d-le

perpendicular. In that case, the second direction is possible to achieve and thus the complete information about the angular position of the point source. This solution is the best for a single point source in the FOV, but for multiple sources is quite difficult to determine right position for right source because of false sources are created during the post-processing. This issue is described in the following section of this thesis and two methods were introduced in the [7] and in the [8].

Detecting a source direction from the 1D LE optics can be relatively straightforward for a single source, as the position of the main focus line will correspond to the angular offset from the centre of the module's optical axis. For multiple sources this can be challenging as sources of the same intensity can produce lines of the same intensity for the same declination. One of the possible solutions to this problem is to place a coded mask in front of the optical module, in the form of a thin strip of material impervious to X-rays, which bypasses the incoming X-rays and produces shading in the sensed image. Due to the high penetration of X-rays through a material, the shading mask must be made of a material that is very absorbent in the X-rays spectrum, such as tungsten. The shading mask creates a gap in the image and it is then possible to determine the second direction of an incident X-ray beam. The coded mask should not affect the sensitivity of the optics too much, it should be as thin as possible, but it must create a gap in the image. An illustration of this situation is given in Figure 4.2.

4.1 Input parameters for simulations

Input parameters for parameters verification are necessary to know, especially used optics, detectors and X–ray sources. Each X–ray Lobster–Eye optics consists of several mirrors which are coated by a reflexive material. The detector has to be able to catch X–ray photons and convert them into the digital signal which can be processed further. Basic parameters of the optics is listed in Table 4.1 and of the detector in Table 4.2.

4.2 Image preparation for the post-processing

Post-processing of two 1D images into a 2D image can be a challenging task especially with more than one source in the FOV. The prerequisites for the images used for the post-processing are following:

- A horizontal image with a gap caused by the coded mask
- A vertical image with the gap caused by the coded mask
- Known mutual orientation of both images (horizontal and vertical)
- If images are not aligned, align them mutually for particular situation, ideally according to the gap in the main line focus
- Deconvolve the the captured images (horizontal and vertical) with their PSF

The theoretical part of the image reconstruction uses two generated 1D images as

Tab. 4.1: Parameters of the examined optics were used in the REX mission and were taken from [44], [45].

Properties	Value
Aperture	54 mm × 54 mm
FOV	1.3° × 1.6°
Focal length	1 065 mm
Radius of convergence	2 130 mm
Foils dimensions	150 mm × 75 mm × 0.35 mm
Number of foils in one sub–module	47
Spacing	0.75 mm
Reflective surface	Au
Reflectivity - energy efficiency	see Figure 2.4
Angular resolution	1.1′ × 1.4′

Tab. 4.2: Parameters of the Timepix detector [41].

Properties	Value
Detector	Timepix
Detection material	500 µm Si detector
Detector resolution	256 px × 256 px
Pixel size	55 µm × 55 µm
Spectral sensitivity	3 − 60 keV

was proposed. These images can contain single or multiple point sources, which the processing task will use.

Input images for post-processing should preferably be square, but this is not required. This condition is necessary for Richardson-Lucy deconvolution [53], [54]. A suitable detector could be, for example, a square detector from the Timepix family, which usually has a size of 256 px × 256 px [41]. The Timepix detector has already been used in combination with 1D Lobster–Eye optics on the successful mission of the nanosatellite VZLUSAT-1 [28], [29] or on the REX mission [45], [52].

One of the elementary examples is in the images in Figure 4.3, where the point source was on the optical axis and in the infinity. This source position causes the gap in the middle of the line, and the primary focus line is centred in the middle of both images, horizontal and vertical. The subsequent data-processing of the image is great to remove the side lobes by deconvolution method with the PSF of the optical module without the central gap. The PSF is visualised in Figure 4.4. This kind of PSF is beneficial for the close-centred line focuses where its deconvolution method produces proper results.

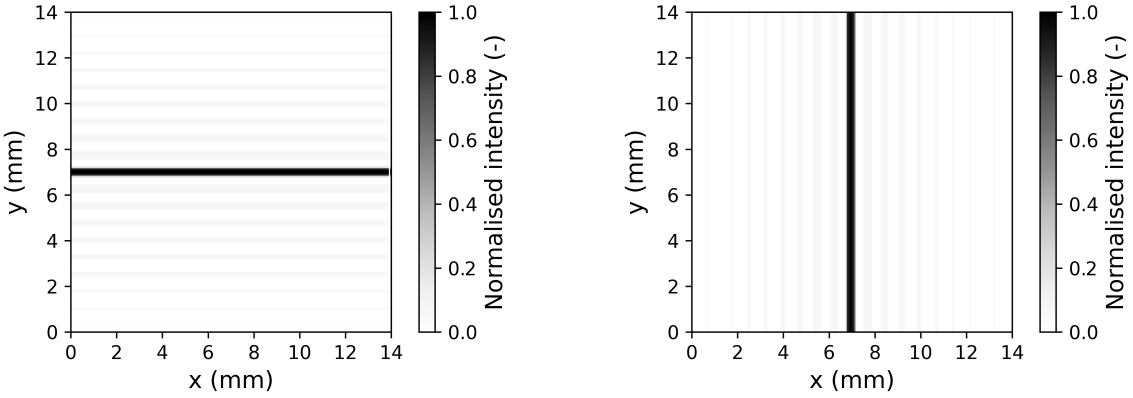

(a) Horizontal optics (b) Vertical optics

Fig. 4.3: Simulation results of two 1D Lobster–Eye X-ray optics generated by PyXLA software. The optics were oriented horizontally and vertically with combination of two Timepix detectors.

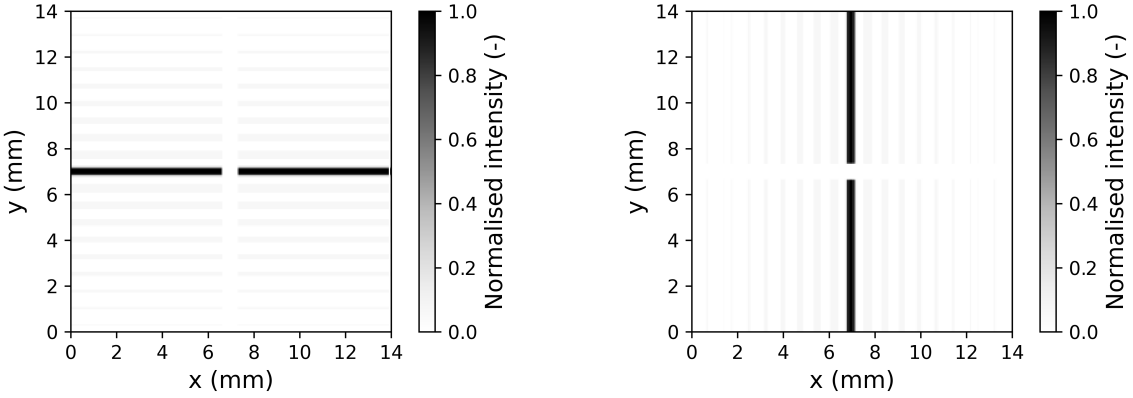

(a) Horizontal module (b) Vertical module

Fig. 4.4: Point spread function of the proposed optics; for horizontal and vertical type of Lobster–Eye optics including gap produced by a thin strip placed in front of the optics

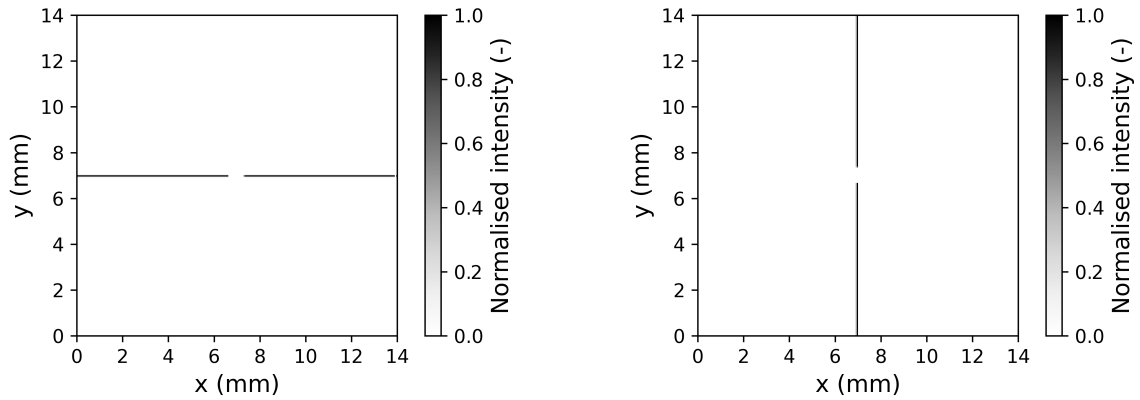

(a) Horizontal module

(b) Vertical module

Fig. 4.5: Deconvoluted line focuses for horizontal and vertical images are shown for one point source with a gap caused by the coded mask

4.3 Point sources identification with masking

The idea about the data-processing from two 1D Lobster–Eye optics was introduced by the author of the thesis at the Society of Photographic Instrumentation Engineers (SPIE) conference in 2017 [7]. The initial algorithm based on the binary mask and matrix multiplication was introduced there and is presented and concluded in the following sections.

For introduction, the processing was used the modelled detector from Timepix family as is listed in Table 4.2 with resolution of 256 px × 256 px and prepared input images as was mentioned in section 4.2. The proposed algorithm is based on the mathematical operations and the binary mask for identifying the images' virtual and right points, especially if more than one source is in the FOV. The processing consists of the following steps:

- Image alignment and their deconvolution with predefined PSF – see section 4.2
- Potential position of sources – Matrix multiplication of horizontal image with the vertical to create the image with the probable position of sources
- Creation of the binary mask based on the gaps caused the coded mask
- Multiplication of the image with potential position of sources and with the binary mask
- Identify the true sources

4.3.1 Alignment and deconvolution of the input images

As was mentioned in section 4.2, the alignment and deconvolution process is crucial for the successful image reconstruction from two 1D Lobster–Eye optics. This processing stage requires memorizing if the input images were rectangular instead of squared. This condition is essential for the deconvolution, which requires the squared image and matrix multiplication. Matrix multiplication can be done with rectangular detector, but the second one must be rotated by 90° to fulfil the condition for it $H_x = V_y$. After that, the final image resolution depends on the arrangement of the detectors and is $H_y \times V_x$. Definition of the parameters and symbols of input images are in Table 4.3 and coordinates of all pixels for horizontal image **H** and for vertical image **V** are in Equation 4.1.

Tab. 4.3: Definition of parameters of input images.

Properties	Horizontal	Vertical
Image marking	**H**	**V**
Dimension X	V_x	H_x
Dimension Y	V_y	H_y
Coordinates	$V_{k,l}$	$H_{m,n}$
Number of line focuses	n_H	n_V

$$\mathbf{H} = \begin{pmatrix} H_{1,1} & H_{1,2} & H_{1,3} & \dots & H_{1,l} \\ H_{2,1} & H_{2,2} & H_{2,3} & \dots & H_{2,l} \\ \vdots & \vdots & \vdots & \ddots & \vdots \\ H_{k,1} & H_{k,2} & H_{k,3} & \dots & H_{k,l} \end{pmatrix}, \quad \mathbf{V} = \begin{pmatrix} V_{1,1} & V_{1,2} & V_{1,3} & \dots & V_{1,n} \\ V_{2,1} & V_{2,2} & V_{2,3} & \dots & V_{2,n} \\ \vdots & \vdots & \vdots & \ddots & \vdots \\ V_{m,1} & V_{m,2} & V_{m,3} & \dots & V_{m,n} \end{pmatrix} \tag{4.1}$$

4.3.2 Potential position of sources

The next step in data processing is to create the image with potential position of sources. This phase includes matrix multiplication as states in Equation 4.2.

$$\mathbf{I} = \mathbf{H} \times \mathbf{V} \tag{4.2}$$

Equation 4.2 uses symbols where **I** is resulting output 2D image, **H** is input 1D image with horizontal lines and **V** is input 1D image with vertical lines. The resulting image **I** contains all combinations of line focuses in both images. The number of potential sources is given by number of line focuses in each image as $n_H n_V$.

4.3.3 Binary mask creation

The penultimate step in the processing is a creation of a binary mask according to input images **H** and **V**, especially with the knowledge of the position of the gaps in the line focuses. A particular solution is to multiply both images **H** and **V** pixel by pixel according to Equation 4.3 into the temporary image **A**. The image **A** contains information about the potential position of sources which were given by the gaps. The binary mask is created based on the Equation 4.4 where the threshold value T can be zero, ideally if no more than one gap is on the same line. If this condition is invalid and there is more than one gap on the same line, the threshold T must be set accordingly.

$$\mathbf{A} = \mathbf{H} \cdot \mathbf{V} \tag{4.3}$$

$$\mathbf{B}(x, y) = \begin{cases} 0, & \text{if } \mathbf{A}(x, y) > T \\ 1, & \text{otherwise} \end{cases} \tag{4.4}$$

Equations 4.3 and 4.4 use symbols where **A** is the matrix (image) made by multiplication of element by element, **H** is input 1D image with horizontal line and shade and **V** is input 1D image with vertical stripe and shade, **B** is a binary coding mask based on values from **A**, T is a threshold value for determination of the minimal value for the creation of the binary mask.

4.3.4 Resulting image

The final stage of the reconstruction relies on the finding of real sources produced by two 1D LE optics. The algorithm uses previous partical results from sections 4.3.2 and 4.3.3 and based on the Equation 4.5 produces resulting image **R**, where one example is in Figure 4.6. The reconstruction of only one source is an elementary task, but it works even for more complex situations. Result should only contains real sources which can by observed further by more precise telescopes.

$$\mathbf{R} = \mathbf{I} \cdot \mathbf{B} \tag{4.5}$$

4.4 Localisation of sources with local minima

Localizing sources in the field of view of both optics can be challenging, especially when more than several point sources are captured. In this case, an improved algorithm is required to find the residual of true sources and eliminate the false one from the previously proposed algorithm in section 4.3.

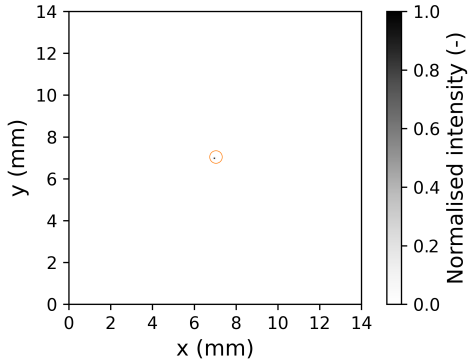

Fig. 4.6: Localisation of true souce in the input 1D images according to Equation 4.5

The author of this thesis proposed this improved algorithm at the conference SPIE with his contribution [8]. The algorithm is based on finding local maxima and then local minima to find true sources in a specified range of valid conditions. The maxima represent the line focuses, and their maxima and local minima represent gaps in the line focuses. According to the previous algorithm in section 4.3, the alignment of both images is required.

4.4.1 Peaks search

Every line focus in input images represents a source, and the point localisation algorithm requires to find all lines. Due to the fact that image can contain multiple focus lines, the local maximum is necessary for identifying and determining their coordinates. For searching local maxima is convenient to use the cross-section of the image if sufficient photons are captured to decrease the processing time. For low photon count is better to sum all rows/columns and search in the sum of the image.

For evaluation of the algorithm, several points were simulated by PyXLA software with input images shown in Figures 4.7 where some points are aligned to the same row or column to demonstrate the purpose of the proposed algorithm.

The simulated situation in Figure 4.7 requires mirroring due to the nature of the 1D optics to reconstruct the position of the sources. If this step is not performed, the two images cannot be used together for more precise source localisation.

Figures in 4.7 represent raw data obtained from simulation which required to be deconvoluted in order to separate focal lines and remove as many side lobes as possible for simplification of sources localisation. Deconvoluted images with Richardson-Lucy deconvolution [53], [54] are shown in Figures 4.8, and there is clearly visible the line focuses.

To identify peaks in the deconvoluted images, it is possible to find local maxima in the cross-section of the image or in the summed rows or columns in the same image in case that low photon count is captured. This part is the same as in the previous case

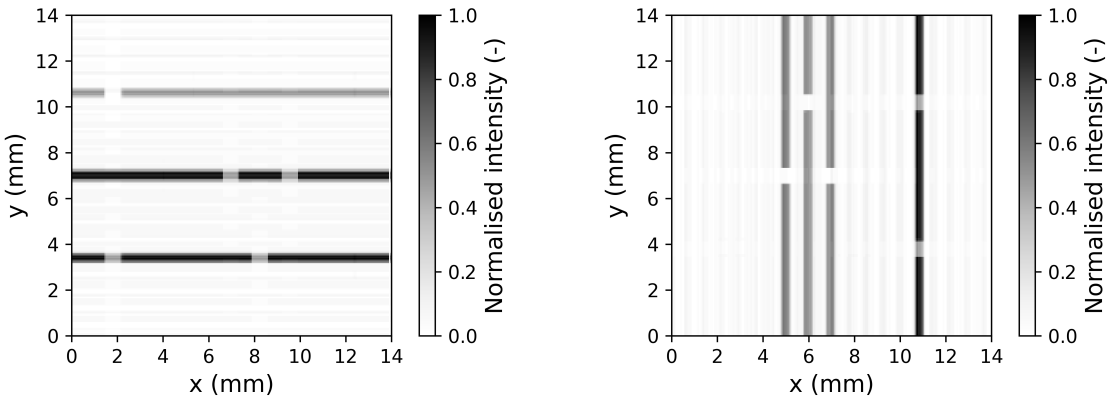

(a) Horizontal (b) Vertical

Fig. 4.7: Images with five sources captured by two independent 1D Lobster–Eye optical modules.

in section 4.4.1, and details can be found there. Due to the fact that input images can be noisy or can contain residuals from the deconvolution, as was suggested in [8], it is recommended to perform moving averages for the cross-section of the summed vector. It produces a smooth vector where local maxima can be found more easily.

When the original plot and plot with moving averages are subtracted, the superposition of two lines can be easily found as shown by the yellow line in Figure 4.9, particularly at 6.6 mm. Peaks in the yellow line represent potential places where sources can be found in the second deconvoluted perpendicular image. In the second image there are shown searches for the local minima, which are represented by gaps in the focal lines. Searching for minima is described in the following chapter 4.4.2.

4.4.2 Minima searching according to peaks

Based on the localised local maxima in Figure 4.9 in section 4.4.1 it is possible to find the complementary minimum in the same 1D image. The minima are caused by the coding mask, which represents a thin strip shape placed in front of the input aperture of the optics. The gap in image 4.10 is related to a particular source according to its position at 6.6 mm. Two methods can achieve the search for minima. The algorithm can search for gaps according to the knowledge of their width (if they are known for sure) or, as well as in the previous case using moving averages to smooth the data. The second method was chosen as a suitable candidate for minima search.

For example, in Figure 4.10 can be determined two minima that there can be two sources, but in this case the minimum at 0.8 mm is a fake one caused by the neighbouring point source at 6.05 mm.

All true sources can be found based on these results, but some can be fake, especially when close to neighbouring. In this case it is required to process the second 1D image and perform the same procedure in both sections 4.4.1 and this 4.4.2. The final

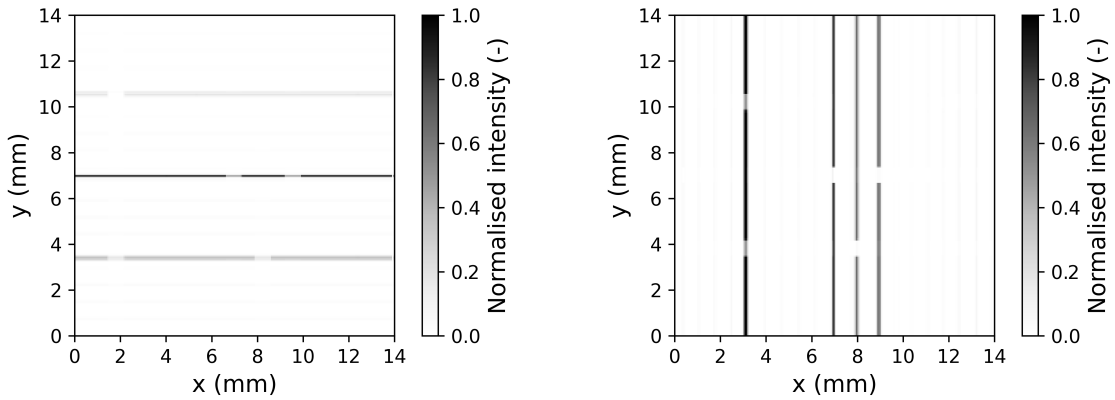

(a) Horizontal (b) Vertical

Fig. 4.8: Deconvoluted images from Figures 4.7 containing five sources captured by two independent 1D Lobster–Eye optics.

determination of all sources is written in the following section 4.4.3.

4.4.3 Position estimation of real sources

The final position of the real sources can be determined in combination with both results from the previous section 4.4.2; for horizontal and vertical images separately. Due to the fact that the position in both resulting images should not be aligned, which can cause false unfavourable position determination, the searched range is applied and was set to 4 px in this case. The matrix multiplication creates the resulting image in Figure 4.11, including several points where it is necessary to identify true and false sources. Localised correct sources are listed in Table 4.4 for each image and are encircled; blue for the horizontal image and green for the vertical one. The final position of real sources is a combination of both images and sources marked as crosses in Figure 4.11.

Based on this process, one image can localise the valid sources successfully, but it can include some false sources. With two 1D images, it is possible to eliminate virtual sources. Table 4.5 presents the position of the original and the localised sources with their original and captured widths and intensity. The width is more expansive because of the properties LE optics, where the Full Width at Half Maximum (FWHM) of the main line focus corresponds to its angular resolution, which is usually large.

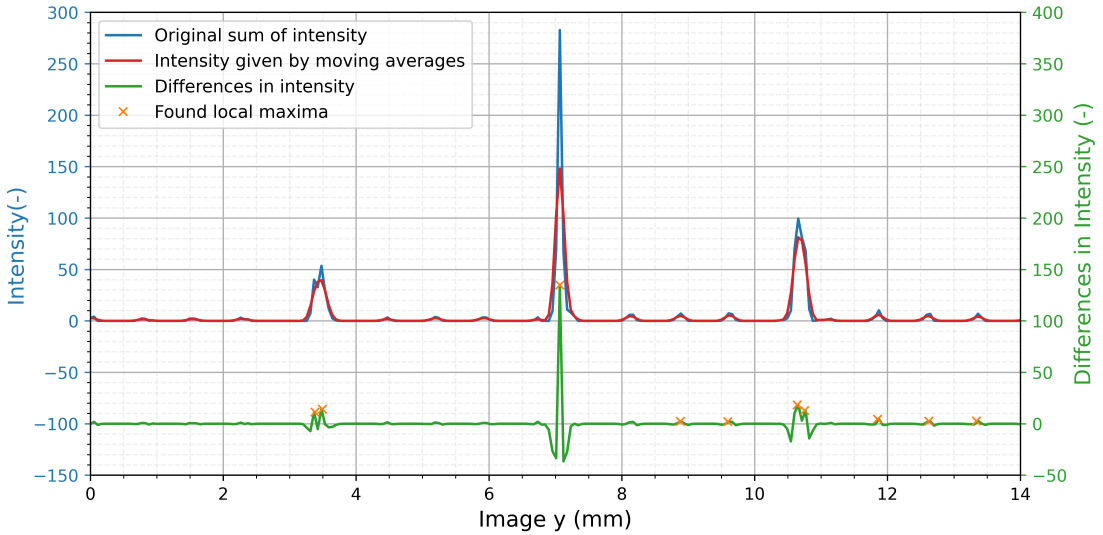

Fig. 4.9: Sum of the all rows for horizontal submodule (blue line) with moving averages (red line) and their differences (green line). Orange crosses on the green curve represent found maxima and suitable point sources.

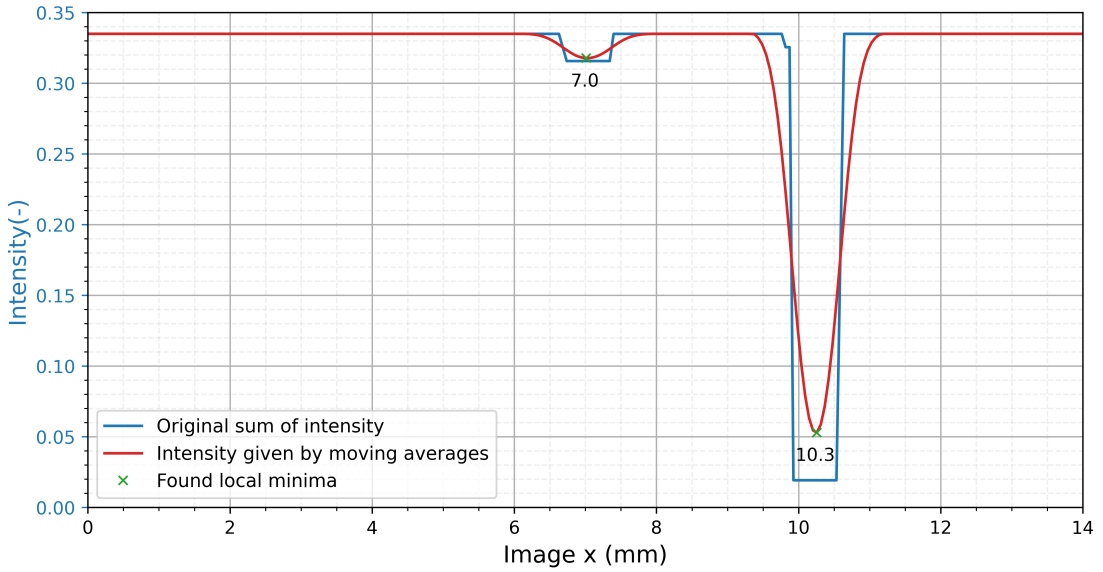

Fig. 4.10: Cross-section of the main peak at 8.1 mm with localised one true source (10.3 mm) and one false (7.0 mm). Blue line represents original data and red line moving averages

Tab. 4.4: Coordinates of localised sources in horizontal and vertical images.

Vertical module		Horizontal module	
x (mm)	**y (mm)**	**x (mm)**	**y (mm)**
14.6	3.16	8.36	0.71
14.6	7.04	1.93	0.71
14.6	10.85	8.36	1.43
9.54	3.16	1.87	1.43
9.54	7.04	8.36	2.2
9.41	3.16	1.87	2.2
9.41	7.04	8.36	3.3
8.29	3.16	1.93	3.3
8.29	7.04	8.36	3.41
7.11	7.04	1.93	3.41
2.44	3.16	8.36	4.45
2.44	10.85	1.87	4.45
1.72	3.16	8.36	5.17
1.72	7.04	1.93	5.17
1.72	10.85	9.68	6.99
0.8	3.16	7.09	6.99
0.8	7.04	1.93	10.56
0.8	10.85	9.68	10.67
		7.09	10.67
		1.93	10.67

Tab. 4.5: Coordinates of the localised five point sources compared to original direction.

Original points		Localised points	
x (°)	**y (°)**	**x (mm)**	**y (mm)**
0	0	7.11	6.99
-0.1	0	9.54	6.99
-0.05	0.15	8.29	3.3
0.2	-0.15	1.72	10.67
0.2	0.15	1.72	3.3

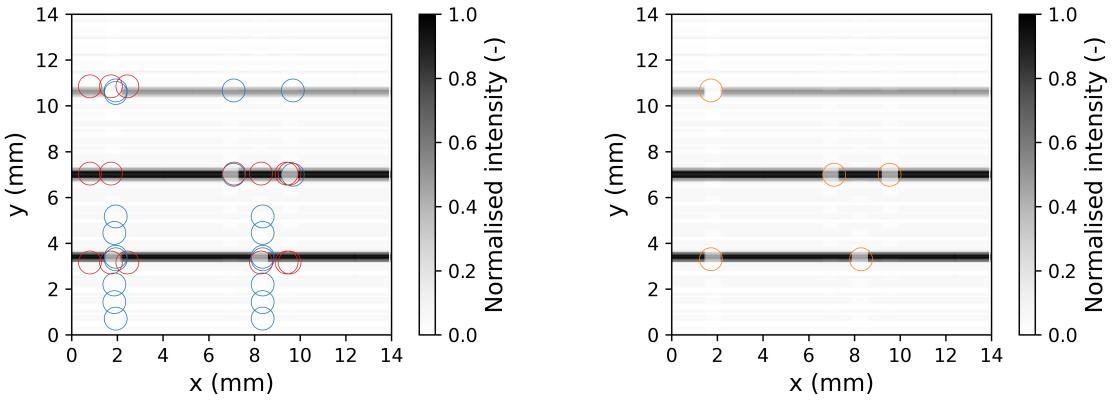

(a) Found points for both modules

(b) Final location of all five sources

Fig. 4.11: Localised sources for both 1D modules and potential sources are encircled, with red circles from the horizontal image and blue circles from the vertical image. Localised all five sources are marked as orange circles.

5 Conclusion of Thesis and Application

Lobster–Eye optics are a very promising type of optics for wide field observations of the X-ray sky. Due to the arrangement of the optics, it is possible to design a telescope with up to 180° FOV. This kind of design can be used as a fast all-sky observer for a future space mission, equipped with an alert system for notifying more precise telescopes that can observe the interesting event in more detail.

Part of this thesis presents the newly developed software by the author of this thesis called Python X-ray-tracing for Lobster-eye Application (PyXLA). It is designed to model a Lobster–Eye optics with defined parameters such as focal length, number of mirrors or the orientation of the mirror stack. This piece of software should allow us to design an optics with demanding parameters and obtain a PSF for further application such as the identification of point sources from two 1D Lobster–Eye optics as proposed in the second part of this thesis.

The feasibility study of identifying point sources such as was stars also proposed in this thesis. The author developed a data processing algorithm based on two 1D Lobster–Eye optics, which consists of two methods of source identification. Both methods are based on the known PSF of the optics, because the line focus are better separated from side reflections or direct rays. A prerequisite for successful identification is the use of a coded mask, in this case a strip of non-penetrable material, e.g. thungsten can be a good candidate, which creates a shadow and makes it possible to identify the direction of the source. Based on the knowledge of the location it is possible to reconstruct the position of the source.

Another method to identify point sources is to look for local minima and maxima and their combination; the gap created by the coded mask and the line focus can be used to identify the position of the sources. This method could use only one 1D optic, but if several sources are close together, the second optic can easily identify them and suppress the false sources well.

Application of the Results

The results of this thesis, such as the developed software PyXLA and the proposed algorithm for point source detection based on two 1D Lobster–Eye optics, can be used for the preparation and the development of future X-ray missions both large by major space agencies as well as small based on minisatellites. The PyXLA can provide valuable data as a PSF for verifying the properties of newly prepared X-ray Lobster–Eye optics and suggesting the correct position of the detector. Another use can be to determine whether or not the intended source can be observed by the optics. This allows faster and more reliable development prior to physical testing.

Due to the difficulty of focusing X-rays, especially at higher energies where X-rays are highly attenuated, it is convenient to use only 1D Lobster–Eye optics to determine the position of sources. This has the disadvantage of requiring more post-processing, but it can achieve fast localisation under the same photon flux if it is equipped in some of the future space missions. The proposed arrangement of two 1D Lobster–Eye modules is completely new and to our knowledge was never described and published prior our study. The novel arrangement represents an alternative in Lobster–Eye optics applications with emphasis on wide-field X-ray sky monitoring and imaging with broader energy coverage up to $20 - 30\,\mathrm{keV}$. This can allow harder X-ray celestial sources to be monitored and exploited.

References

[1] H. Wolter, "Spiegelsysteme streifenden Einfalls als abbildende Optiken für Röntgenstrahlen," *Annalen der Physik*, vol. 445, no. 1-2, pp. 94–114, 1952, ISSN: 00033804. DOI: 10.1002/andp.19524450108.

[2] M. C. Weisskopf, H. D. Tananbaum, L. P. Van Speybroeck, and S. L. O'Dell, "Chandra X-ray Observatory (CXO): overview," *Proc. SPIE Vol. 4012*, vol. 4012, no. 4, pp. 2–16, 2000. DOI: 10.1117/12.391545. arXiv: 0004127 [astro-ph].

[3] D. Barret, K. Nandra, X. Barcons, *et al.*, "Athena+: The first Deep Universe X-ray Observatory," *ArXiv e-prints*, vol. 1310, p. 7, 2013.

[4] W. Schmidt, "A proposed X-ray focusing device with wide field of view for use in X-ray astronomy," *Nuclear Instruments and Methods*, vol. 127, no. 2, pp. 285–292, Aug. 1975, ISSN: 0029554X. DOI: 10.1016/0029-554X(75)90501-7.

[5] J. R. P. Angel, "Lobster eyes as X-ray telescopes," *The Astrophysical Journal*, vol. 233, p. 364, Oct. 1979, ISSN: 0004-637X. DOI: 10.1086/157397.

[6] W. Yuan, C. Zhang, H. Feng, *et al.*, "Einstein probe - a small mission to monitor and explore the dynamic x-ray universe," Jun. 2015.

[7] O. Nentvich, V. Stehlikova, M. Urban, R. Hudec, and L. Sieger, "Data processing from lobster eye type optics," vol. 10235, 2017, ISBN: 9781510609716. DOI: 10.1117/12.2265724.

[8] O. Nentvich, M. Urban, M. Blazek, A. Inneman, R. Hudec, and L. Sieger, "Lobster eye optics: Position determination based on 1d optics with simple code mask," vol. 11108, 2019, ISBN: 9781510629097. DOI: 10.1117/12.2528505.

[9] L. Dressel, *Wide Field Camera 3 Instrument Handbook, Version 14.0*. Baltimore: STScI, 2022.

[10] M. D. Lallo, "Experience with the hubble space telescope: 20 years of an archetype," *Optical Engineering*, vol. 51, p. 011 011, 1 Feb. 2012, ISSN: 0091-3286. DOI: 10.1117/1.OE.51.1.011011.

[11] E. Furlan, M. McClure, N. Calvet, *et al.*, "Spitzer irs spectra and envelope models of class i protostars in taurus," *The Astrophysical Journal Supplement Series*, vol. 176, pp. 184–215, 1 May 2008, ISSN: 0067-0049. DOI: 10.1086/527301.

[12] C. A. Poteet, S. T. Megeath, D. M. Watson, *et al.*, "A spitzer infrared spectrograph detection of crystalline silicates in a protostellar envelope," *The Astrophysical Journal*, vol. 733, p. L32, 2 Jun. 2011, ISSN: 2041-8205. DOI: 10.1088/2041-8205/733/2/L32.

[13] J. P. Gardner, J. C. Mather, M. Clampin, *et al.*, "The james webb space telescope," *Space Science Reviews*, vol. 123, pp. 485–606, 4 Apr. 2006, ISSN: 0038-6308. DOI: 10.1007/s11214-006-8315-7.

[14] K. Grasha, D. Calzetti, A. Adamo, *et al.*, "The spatial relation between young star clusters and molecular clouds in m51 with legus," *Monthly Notices of the Royal Astronomical Society*, vol. 483, pp. 4707–4723, 4 Mar. 2019, ISSN: 0035-8711. DOI: 10.1093/mnras/sty3424.

[15] J. García and T. R. Kallman, "X-ray reflected spectra from accretion disk models. i. constant density atmospheres," *The Astrophysical Journal*, vol. 718, pp. 695–706, 2 Aug. 2010, ISSN: 0004-637X. DOI: 10.1088/0004-637X/718/2/695.

[16] G. Piotto, A. P. Milone, L. R. Bedin, *et al.*, "The hubble space telescope uv legacy survey of galactic globular clusters. i. overview of the project and detection of multiple stellar populations," *The Astronomical Journal*, vol. 149, p. 91, 3 Feb. 2015, ISSN: 1538-3881. DOI: 10.1088/0004-6256/149/3/91.

[17] A. G. Riess, S. Casertano, W. Yuan, *et al.*, "Milky way cepheid standards for measuring cosmic distances and application to gaia dr2: Implications for the hubble constant," *The Astrophysical Journal*, vol. 861, p. 126, 2 Jul. 2018, ISSN: 1538-4357. DOI: 10.3847/1538-4357/aac82e.

[18] D. T. Attwood, *Soft x-rays and extreme ultraviolet radiation: principles and applications*. Cambridge ; New York: Cambridge University Press, 2000, 470 pp., ISBN: 9780521652148.

[19] N. Gehrels and P. Mészáros, "Gamma-ray bursts," *Science*, vol. 337, pp. 932–936, 6097 Aug. 2012, ISSN: 0036-8075. DOI: 10.1126/science.1216793.

[20] S. D. Shastri and N. Moldovan, "Submicron focusing of high-energy x-rays with silicon saw-tooth refractive lenses: Fabrication and aberrations," *Optics Express*, vol. 28, p. 36 505, 24 Nov. 2020, ISSN: 1094-4087. DOI: 10.1364/OE.405566.

[21] B. Cederström, R. N. Cahn, M. Danielsson, M. Lundqvist, and D. R. Nygren, "Focusing hard x-rays with old lps," *Nature*, vol. 404, pp. 951–951, 6781 Apr. 2000, ISSN: 0028-0836. DOI: 10.1038/35010190.

[22] C. Ribbing, B. r. Cederstr m, and M. Lundqvist, "Microfabrication of saw-tooth refractive x-ray lenses in low- Z materials," *Journal of Micromechanics and Microengineering*, vol. 13, no. 5, pp. 714–720, Sep. 1, 2003, ISSN: 0960-1317, 1361-6439. DOI: 10.1088/0960-1317/13/5/325.

[23] M. Howells, C. Jacobsen, T. Warwick, and A. V. den Bos, "Principles and applications of zone plate x-ray microscopes," in Springer New York, 2007, pp. 835–926. DOI: 10.1007/978-0-387-49762-4_13.

[24] D. H. Lumb, "X-ray multi-mirror mission (xmm-newton) observatory," *Optical Engineering*, vol. 51, p. 011 009, 1 Feb. 2012, ISSN: 0091-3286. DOI: 10.1117/1.OE.51.1.011009.

[25] D. Castelvecchi, "Space telescope to chart first map of the universe in high-energy x-rays," *Nature*, vol. 570, pp. 149–150, 7760 Jun. 2019, ISSN: 0028-0836. DOI: 10.1038/d41586-019-01831-1.

[26] B. Henke, E. Gullikson, and J. Davis, "X-ray interactions: Photoabsorption, scattering, transmission, and reflection at e = 50-30,000 ev, z = 1-92," *Atomic Data and Nuclear Data Tables*, vol. 54, pp. 181–342, 2 Jul. 1993, ISSN: 0092640X. DOI: 10.1006/adnd.1993.1013.

[27] A. C. Thompson, J. Kirz, D. T. Attwood, *et al.*, *X-Ray Data Booklet*, Third. Berkeley, California: Lawrence Berkeley National Laboratory, University of California, 2009.

[28] T. Baca, M. Platkevic, J. Jakubek, *et al.*, "Miniaturized x-ray telescope for vzlusat-1 nanosatellite with timepix detector," *Journal of Instrumentation*, vol. 11, pp. C10007–C10007, 10 Oct. 2016, ISSN: 1748-0221. DOI: 10.1088/1748-0221/11/10/C10007.

[29] M. Urban, O. Nentvich, V. Stehlikova, T. Baca, V. Daniel, and R. Hudec, "Vzlusat-1: Nanosatellite with miniature lobster eye x-ray telescope and qualification of the radiation shielding composite for space application," *Acta Astronautica*, vol. 140, pp. 96–104, Nov. 2017, ISSN: 00945765. DOI: 10.1016/j.actaastro.2017.08.004.

[30] T. Baca, M. Jilek, I. Vertat, *et al.*, "Timepix in leo orbit onboard the vzlusat-1 nanosatellite: 1-year of space radiation dosimetry measurements," *Journal of Instrumentation*, vol. 13, pp. C11010–C11010, 11 Nov. 2018, ISSN: 1748-0221. DOI: 10.1088/1748-0221/13/11/C11010.

[31] W. Yuan, C. Zhang, Z. Ling, *et al.*, "Einstein probe: A lobster-eye telescope for monitoring the x-ray sky," J.-W. A. den Herder, K. Nakazawa, and S. Nikzad, Eds., SPIE, Jul. 2018, p. 76, ISBN: 9781510619517. DOI: 10.1117/12.2313358.

[32] P. Kirkpatrick and A. V. Baez, "Formation of optical images by x-rays," *Journal of the Optical Society of America*, vol. 38, p. 766, 9 Sep. 1948, ISSN: 0030-3941. DOI: 10.1364/JOSA.38.000766. [Online]. Available: https://www.osapublishing.org/abstract.cfm?URI=josa-38-9-766.

[33] R. Hudec, "Kirkpatrick-Baez (KB) and Lobster Eye (LE) Optics for Astronomical and Laboratory Applications," *X-Ray Optics and Instrumentation*, vol. 2010, pp. 1–39, 2010, ISSN: 1687-7632. DOI: 10.1155/2010/139148.

[34] *Curved mirror optics*, German. [Online]. Available: http://www.x-ray-optics.de/index.php/en/types-of-optics/reflecting-optics/curved-mirrors (visited on 02/06/2023).

[35] A. G. Peele, H. Lyngsjo, R. M. Crocker, J. Markham, N. Bannister, and K. A. Nugent, "Modeling of the Lobster-ISS x-ray telescope in orbit," G. Hasinger and M. J. L. Turner, Eds., Oct. 2004, p. 232. DOI: 10.1117/12.550975.

[36] R. Hudec, L. Pína, A. Inneman, and L. Švéda, "Variable X–ray sky with Lobster Eye Telescopes," *Nuclear Physics B - Proceedings Supplements*, vol. 132, pp. 320–323, Jun. 2004, ISSN: 09205632. DOI: 10.1016/j.nuclphysbps.2004.04.057.

[37] L. Sveda, V. Semencova, A. Inneman, L. Pina, and R. Hudec, "Hybrid lobster optic," G. A. Kyrala, J.-C. J. Gauthier, C. A. MacDonald, and A. M. Khounsary, Eds., Aug. 2005, p. 591 803. DOI: 10.1117/12.620247.

[38] O. Nentvich, M. Urban, V. Stehlikova, L. Sieger, and R. Hudec, "Lobster eye x-ray optics: Data processing from two 1d modules," *Contributions of the Astronomical Observatory Skalnaté Pleso*, vol. 47, pp. 178–183, 2 2017.

[39] R. Hudec and V. Simon, "Cvs astrophysics with lobster and esa loft," Sissa Medialab, Apr. 2017, p. 075. DOI: 10.22323/1.255.0075.

[40] O. Nentvich, M. Urban, and R. Hudec, "Pyxla: Python x-ray-tracing for lobster-eye application," *Journal of Optics*, Mar. 2023, ISSN: 2040-8978. DOI: 10.1088/2040-8986/acc2cc.

[41] T. Poikela, J. Plosila, T. Westerlund, *et al.*, "Timepix3: A 65k channel hybrid pixel readout chip with simultaneous toa/tot and sparse readout," *Journal of Instrumentation*, vol. 9, pp. C05013–C05013, 05 May 2014, ISSN: 1748-0221. DOI: 10.1088/1748-0221/9/05/C05013.

[42] M. Urban and D. Doubravová, "Timepix3: Temperature influence on x-ray measurements in counting mode with si sensor," *Radiation Measurements*, vol. 141, p. 106 535, Feb. 2021, ISSN: 13504487. DOI: 10.1016/j.radmeas.2021.106535.

[43] M. Urban, O. Nentvich, L. Marek, R. Hudec, and L. Sieger, "Timepix3: Temperature influence on radiation energy measurement with si sensor," *Sensors*, vol. 23, p. 2201, 4 Feb. 2023, ISSN: 1424-8220. DOI: 10.3390/s23042201.

[44] R. Hudec, L. Pina, V. Marsikova, O. Nentvich, M. Urban, and A. Inneman, "Lobster eye x–ray optics for astrophysics: Recent status," *Contributions of the Astronomical Observatory Skalnate Pleso*, vol. 48, pp. 456–465, 3 2018.

[45] M. Urban, O. Nentvich, T. Báča, *et al.*, "Rex: X-ray experiment on the water recovery rocket," *Acta Astronautica*, vol. 184, pp. 1–10, Jul. 2021, ISSN: 00945765. DOI: 10.1016/j.actaastro.2021.03.019.

[46] X. Llopart, R. Ballabriga, M. Campbell, L. Tlustos, and W. Wong, "Timepix, a 65k programmable pixel readout chip for arrival time, energy and/or photon counting measurements," *Nuclear Instruments and Methods in Physics Research Section A: Accelerators, Spectrometers, Detectors and Associated Equipment*, vol. 581, pp. 485–494, 1-2 Oct. 2007, ISSN: 01689002. DOI: 10.1016/j.nima.2007.08.079.

[47] V. Tichý, R. Hudec, and M. Barbera, "Analytical description of lobster eye and similar multi-foil optics," R. Hudec and L. Pina, Eds., May 2015, p. 95100C. DOI: 10.1117/12.2178678. [Online]. Available: http://proceedings.spiedigitallibrary.org/proceeding.aspx?doi=10.1117/12.2178678.

[48] V. Tichý, M. Barbera, R. Hudec, and R. Willingale, "Effective collecting area of lobster eye optics and optimal value of effective angle," *Experimental Astronomy*, vol. 47, pp. 161–175, 1-2 Apr. 2019, ISSN: 0922-6435. DOI: 10.1007/s10686-019-09622-2. [Online]. Available: http://link.springer.com/10.1007/s10686-019-09622-2.

[49] V. Tichy, R. Hudec, and S. Nemcová, "Effective algorithm for ray-tracing simulations of lobster eye and similar reflective optical systems," *Experimental Astronomy*, vol. 41, no. 3, pp. 377–392, Jun. 2016, ISSN: 0922-6435. DOI: 10.1007/s10686-016-9493-2.

[50] V. Daniel, A. Inneman, I. Vertat, *et al.*, "In-orbit commissioning of czech nanosatellite vzlusat-1 for the qb50 mission with a demonstrator of a miniaturised lobster-eye x-ray telescope and radiation shielding composite materials," *Space Science Reviews*, vol. 215, p. 40, 5 Aug. 2019, ISSN: 0038-6308. DOI: 10.1007/s11214-019-0589-7.

[51] L. Pina, R. Hudec, A. Inneman, *et al.*, "Multi-foil x-ray optics tests at panter: Preliminary results," *Contributions Of The Astronomical Observatory Skalnate Pleso*, vol. 48, pp. 466–475, 3 2018, ISSN: 1335-1842.

[52] V. Dániel, R. Hudec, T. Baca, *et al.*, "Rex le x-ray telescope experiment overview," R. Hudec and L. Pina, Eds., SPIE, Apr. 2019, p. 5, ISBN: 9781510627307. DOI: 10.1117/12.2527288.

[53] W. H. Richardson, "Bayesian-based iterative method of image restoration*," *Journal of the Optical Society of America*, vol. 62, p. 55, 1 Jan. 1972, ISSN: 0030-3941. DOI: 10.1364/JOSA.62.000055. [Online]. Available: https://www.osapublishing.org/abstract.cfm?URI=josa-62-1-55.

[54] L. B. Lucy, "An iterative technique for the rectification of observed distributions," *The Astronomical Journal*, vol. 79, p. 745, Jun. 1974, ISSN: 00046256. DOI: 10.1086/111605. [Online]. Available: http://adsabs.harvard.edu/cgi-bin/bib_query?1974AJ.....79..745L.

A Author's Publications and Related Works

A.1 Articles Related to PhD Thesis

Impacted Journals in WoS

1. **O. Nentvich**, M. Urban, and R. Hudec, "Pyxla: Python x-ray-tracing for lobster-eye application," *Journal of Optics*, Mar. 2023, ISSN: 2040-8978. DOI: 10.1088/2040-8986/acc2cc.
2. **O. Nentvich**, M. Urban, V. Stehlikova, L. Sieger, and R. Hudec, "Lobster eye x-ray optics: Data processing from two 1d modules," *Contributions Of The Astronomical Observatory Skalnate Pleso*, vol. 47, pp. 178–183, 2 2017, ISSN: 1335-1842.
3. T. Baca, M. Platkevic, J. Jakubek, *et al.*, "Miniaturized x-ray telescope for vzlusat-1 nanosatellite with timepix detector," *Journal of Instrumentation*, vol. 11, Oct. 2016, 18th International Workshop on Radiation Imaging Detectors, Barcelona, SPAIN, JUL 03-07, 2016, ISSN: 1748-0221.
4. L. Pina, R. Hudec, A. Inneman, *et al.*, "Multi-foil x-ray optics tests at panter: Preliminary results," *Contributions Of The Astronomical Observatory Skalnate Pleso*, vol. 48, pp. 466–475, 3 2018, ISSN: 1335-1842.
5. V. Daniel, A. Inneman, I. Vertat, *et al.*, "In-orbit commissioning of czech nanosatellite vzlusat-1 for the qb50 mission with a demonstrator of a miniaturised lobster-eye x-ray telescope and radiation shielding composite materials," *Space Science Reviews*, vol. 215, 5 Aug. 2019, ISSN: 0038-6308.
6. M. Urban, **O. Nentvich**, V. Stehlikova, T. Baca, V. Daniel, and R. Hudec, "Vzlusat-1: Nanosatellite with miniature lobster eye x-ray telescope and qualification of the radiation shielding composite for space application," *Acta Astronautica*, vol. 140, pp. 96–104, Nov. 2017, ISSN: 0094-5765.
7. M. Urban, **O. Nentvich**, T. Baca, *et al.*, "Rex: X-ray experiment on the water recovery rocket," *Acta Astronautica*, vol. 184, pp. 1–10, Jul. 2021, ISSN: 0094-5765.

Conference Proceedings in WOS

1. **O. Nentvich**, V. Stehlikova, M. Urban, R. Hudec, and L. Sieger, "Data processing from lobster eye type optics," R. Hudec and L. Pina, Eds., Conference

on EUV and X-ray Optics - Synergy between Laboratory and Space V, Prague, Czech Republic, APR 26-27, 2017, vol. 10235, Spie-int soc Optical Engineering, 2017, ISBN: 978-1-5106-0971-6; 978-1-5106-0972-3.

2. **O. Nentvich**, M. Urban, M. Blazek, R. I. Adolf, Hudec, and L. Sieger, "Lobster eye optics: Position determination based on 1d optics with a simple coded mask," A. M. Khounsary, S. Goto, and C. Morawe, Eds., Conference on Advances in X-Ray/EUV Optics and Components XIV, San Diego, CA, AUG 14-15, 2019, vol. 11108, Spie-int soc Optical Engineering, 2019, ISBN: 978-1-5106-2910-3.
3. V. Daniel, R. Hudec, T. Baca, *et al.*, "Rex le x-ray telescope experiment overview," R. Hudec and L. Pina, Eds., Conference on EUV and X-Ray Optics - Synergy between Laboratory and Space VI, Prague, Czech Republic, APR 03-04, 2019, vol. 11032, Spie-int soc Optical Engineering, 2019, ISBN: 978-1-5106-2731-4.

A.2 Articles not Directly Related to PhD Thesis

Impacted Journals in WOS

1. **O. Nentvich**, M. Urban, V. Stehlikova, L. Sieger, and A. Inneman, "Vzlusat-1: Health monitoring system, preliminary results," *Astronomische Nachrichten*, vol. 339, pp. 397–402, 5, SI Jun. 2018, ISSN: 0004-6337.
2. M. Urban, **O. Nentvich**, V. Stehlikova, and L. Sieger, "Detection of x-ray spectra and images by timepix," *Contributions Of The Astronomical Observatory Skalnate Pleso*, vol. 47, pp. 151–156, 2 2017, ISSN: 1335-1842.
3. V. Stehlikova, M. Urban, **O. Nentvich**, V. Daniel, L. Sieger, and J. Tutt, "Hard x-ray vela supernova observation on rocket experiment wrx-r," *Contributions Of The Astronomical Observatory Skalnate Pleso*, vol. 47, pp. 165–169, 2 2017, ISSN: 1335-1842.
4. V. Stehlikova, A. .-. Probst, **O. Nentvich**, *et al.*, "Study of multiple layers coatings for x-ray mirrors," *Contributions Of The Astronomical Observatory Skalnate Pleso*, vol. 48, pp. 488–497, 3 2018, ISSN: 1335-1842.
5. R. Hudec, L. Pina, V. Marsikova, **O. Nentvich**, A. U. M., and Inneman, "Lobster eye x-ray optics for astrophysics: Recent status," *Contributions Of The Astronomical Observatory Skalnate Pleso*, vol. 48, pp. 456–465, 3 2018, ISSN: 1335-1842.
6. R. Hudec, L. Pina, V. Marsikova, **O. Nentvich**, A. U. M., and Inneman, "Kirkpatrick baez x-ray optics for astrophysics: Recent status," *Contributions Of The Astronomical Observatory Skalnate Pleso*, vol. 48, pp. 437–445, 3 2018, ISSN: 1335-1842.
7. M. Urban, **O. Nentvich**, V. Stehlikova, L. Sieger, and L. Mikulickova, "Outgassing monitor on vzlusat-1: Preliminary results," *Astronomische Nachrichten*, vol. 339, pp. 367–370, 5, SI Jun. 2018, ISSN: 0004-6337.
8. V. Stehlikova, M. Urban, **O. Nentvich**, and L. Sieger, "Radiation resistance monitor on vzlusat-1: Preliminary results," *Astronomische Nachrichten*, vol. 339, pp. 382–385, 5, SI Jun. 2018, ISSN: 0004-6337.
9. T. Baca, M. Jilek, I. Vertat, *et al.*, "Timepix in leo orbit onboard the vzlusat-1 nanosatellite: 1-year of space radiation dosimetry measurements," *Journal of Instrumentation*, vol. 13, Nov. 2018, 20th International Workshop on Radiation Imaging Detectors, Sundsvall, Sweden, JUN 24-28, 2018, ISSN: 1748-0221.
10. M. Urban, D. Doubravova, and **O. Nentvich**, "Thermal vacuum testing of timepix3 detector," *Journal of Instrumentation*, vol. 15, 3 Mar. 2020, 21st International Workshop on Radiation Imaging Detectors, Crete, Greece, JUL 07-12, 2019, ISSN: 1748-0221.
11. L. Sieger, **O. Nentvich**, and M. Urban, "Satellite temperature measurement in leo and improvement method of temperature sensors calibration based on the

measured data," *Astronomische Nachrichten*, vol. 340, pp. 652–657, 7, SI Aug. 2019, ISSN: 0004-6337.
12. M. Urban, **O. Nentvich**, L. Marek, R. Hudec, and L. Sieger, "Timepix3: Temperature influence on radiation energy measurement with si sensor," *Sensors*, vol. 23, p. 2201, 4 Feb. 2023, ISSN: 1424-8220. DOI: 10.3390/s23042201.
13. M. Urban, O. Nentvich, L. Marek, D. Hladik, R. Hudec, and L. Sieger, "Timepix3: Compensation of thermal distortion of energy measurement," *Sensors*, vol. 23, p. 3362, 6 Mar. 2023, ISSN: 1424-8220. DOI: 10.3390/s23063362.

Conference Proceedings in WOS

1. V. Dániel, L. Pína, A. Inneman, *et al.*, "Terrestrial gamma-ray flashes monitor demonstrator on cubesat," vol. 9978, 2016, ISBN: 9781510603479.
2. V. Daniel, A. Inneman, L. Pina, *et al.*, "X-ray lobster eye all-sky monitor for rocket experiment," R. Hudec and L. Pina, Eds., Conference on EUV and X-ray Optics - Synergy between Laboratory and Space V, Prague, Czech Republic, APR 26-27, 2017, vol. 10235, Spie-int soc Optical Engineering, 2017, ISBN: 978-1-5106-0971-6; 978-1-5106-0972-3.
3. T. Baca, M. Jilek, I. Vertat, *et al.*, "Timepix in leo orbit onboard the vzlusat-1 nanosatellite: 1-year of space radiation dosimetry measurements," *Journal of Instrumentation*, vol. 13, Nov. 2018, 20th International Workshop on Radiation Imaging Detectors, Sundsvall, Sweden, JUN 24-28, 2018, ISSN: 1748-0221.
4. V. Daniel, M. Urban, **O. Nentvich**, and V. Stehlikova, "Vzlusat-1: Verification of new materials and technologies for space," T. S. Pagano, Ed., Conference on CubeSats and NanoSats for Remote Sensing, San Diego, CA, AUG 31, 2016, vol. 9978, Spie-int soc Optical Engineering, 2016, ISBN: 978-1-5106-0347-9; 978-1-5106-0348-6.
5. M. Urban, **O. Nentvich**, V. Stehlikova, and L. Sieger, "Uncooled spectrometer for x-ray astrophysics," R. Hudec and L. Pina, Eds., Conference on EUV and X-ray Optics - Synergy between Laboratory and Space V, Prague, Czech Republic, APR 26-27, 2017, vol. 10235, Spie-int soc Optical Engineering, 2017, ISBN: 978-1-5106-0971-6; 978-1-5106-0972-3.
6. V. Stehlikova, M. Urban, **O. Nentvich**, A. Inneman, T. Doehring, and A.-C. Probst, "Study of lobster eye optics with iridium coated x-ray mirrors for a rocket experiment," R. Hudec and L. Pina, Eds., Conference on EUV and X-ray Optics - Synergy between Laboratory and Space V, Prague, Czech Republic, APR 26-27, 2017, vol. 10235, Spie-int soc Optical Engineering, 2017, ISBN: 978-1-5106-0971-6; 978-1-5106-0972-3.
7. L. Mikulickova, L. Pina, A. Inneman, *et al.*, "Optimization of microroughness of replicated x-ray optics," R. Hudec and L. Pina, Eds., Conference on EUV and X-ray Optics - Synergy between Laboratory and Space V, Prague, Czech Republic,

APR 26-27, 2017, vol. 10235, Spie-int soc Optical Engineering, 2017, ISBN: 978-1-5106-0971-6; 978-1-5106-0972-3.

8. M. Urban, **O. Nentvich**, D. Doubravova, *et al.*, "Timepix: Influence of temperature and vacuum on equalisation of x-ray detector and its verification," O. H. Siegmund, Ed., Conference on UV, X-Ray, and Gamma-Ray Space Instrumentation for Astronomy XXI held at SPIE Optical Engineering + Applications Conference, San Diego, CA, AUG 11-13, 2019, vol. 11118, Spie-int soc Optical Engineering, 2019, ISBN: 978-1-5106-2929-5; 978-1-5106-2930-1.
9. A.-C. Probst and A. Et, "Iridium coatings for space based x-ray optics," Biarritz, 2016.

A.3 Recognition by the Scientific Community

Editorship of a Special Issue of the WoS Excerpted Journal

- R. Hudec, M. Urban, **O. Nentvich**, "Special Issue: 16th Integral/Bart Workshop (IBWS)", *Astronomische Nachrichten*, vol.340, no 7, Aug. 2019
- R. Hudec, M. Urban, **O. Nentvich**, "Special Issue: 15th INTEGRAL / BART Workshop", *Astronomische Nachrichten*, vol.339, no 5, Jun. 2018
- R. Hudec, M. Urban, **O. Nentvich**, "Special Issue: 10th International Workshop on Astronomical X—Ray Optics", *Contributions Of The Astronomical Observatory Skalnate Pleso*, vol.48, no 3, Aug. 2018
- M. Urban, **O. Nentvich**, R. Hudec, "Special Issue: 14th INTEGRAL/BART Workshop", *Contributions Of The Astronomical Observatory Skalnate Pleso*, vol. 47, no 2, Aug. 2017

Member of the Local Organising Committee of the International Conferences

- 17th INTEGRAL/BART Workshop 2023
- 16th INTEGRAL/BART Workshop 2019
- 15th INTEGRAL/BART Workshop 2018
- 14th INTEGRAL/BART Workshop 2017
- 13th INTEGRAL/BART Workshop 2016
- 13th International Workshop on Astronomical X-Ray Optics (AXRO) 2022
- 12th International Workshop on Astronomical X-Ray Optics (AXRO) 2019
- 11th International Workshop on Astronomical X-Ray Optics (AXRO) 2018
- 10th International Workshop on Astronomical X-Ray Optics (AXRO) 2017
- 9th International Workshop on Astronomical X-Ray Optics (AXRO) 2016

B Citations of author's publications

Citations of the author's work were extracted from the Web of Science (WOS) First-order self-citations are excluded. The data were gathered on February 14th, 2023 and the author has reached h-index 5.

T. Baca, M. Platkevic, J. Jakubek, A. Inneman, V. Stehlikova, M. Urban, *et al.*, "Miniaturized x-ray telescope for vzlusat-1 nanosatellite with timepix detector," *Journal of Instrumentation*, vol. 11, Oct. 2016, 18th International Workshop on Radiation Imaging Detectors, Barcelona, SPAIN, JUL 03-07, 2016, ISSN: 1748-0221

1. V. Simon and R. Hudec, "Perspectives of the lobster-eye monitor in the soft x-ray observing the galactic center region," English, *Journal of High Energy Astrophysics*, vol. 35, pp. 69–76, Jan. 2022.
2. V. V. Lider, "Grazing-incidence focusing optics for x-ray telescopes (review)," English, *Instruments and Experimental Techniques*, vol. 65, no. 2, pp. 191–217, Jan. 2022.
3. M. Ruffenach, S. Bourdarie, B. Bergmann, S. Gohl, J. Mekki, and J. Vaille, "A new technique based on convolutional neural networks to measure the energy of protons and electrons with a single timepix detector," English, *IEEE Transactions on Nuclear Science*, vol. 68, no. 8, 1-3, pp. 1746–1753, Jan. 2021.
4. R. Filgas, M. Malich, T. Kuwahara, *et al.*, "Risepix — a timepix-based radiation monitor telescope onboard the risesat satellite," English, *Astronomische Nachrichten*, vol. 340, no. 7, SI, pp. 674–680, Jan. 2019.
5. V. Tichy, M. Barbera, R. Hudec, and R. Willingale, "Effective collecting area of lobster eye optics and optimal value of effective angle," English, *Experimental Astronomy*, vol. 47, no. 1-2, pp. 161–175, Jan. 2019.
6. W. Furnell, A. Shenoy, E. Fox, and P. Hatfield, "First results from the lucid-timepix spacecraft payload onboard the techdemosat-1 satellite in low earth orbit," English, *Advances In Space Research*, vol. 63, no. 5, pp. 1523–1540, Jan. 2019.
7. P. Hatfield, W. Furnell, A. Shenoy, *et al.*, "Iris opens pupils' eyes to real space research," English, *Astronomy & Geophysics*, vol. 60, no. 1, pp. 22–24, Jan. 2019.
8. R. Hudec, "X/euv and uv optics for miniature cube satellites payloads," English, in *EUV and X-Ray Optics: Synergy Between Laboratory and Space VI*, vol. 11032,

1000 20TH ST, PO BOX 10, BELLINGHAM, WA 98227-0010 USA: SPIE-INT SOC OPTICAL ENGINEERING, 2019.
9. P. Hatfield, W. Furnell, A. Shenoy, E. Fox, R. Parker, and L. Thomas, "The lucid-timepix spacecraft payload and the cern school educational programme," English, *Journal of Instrumentation*, vol. 13, Jan. 2018.
10. V. Tichy and R. Willingale, "Optimization of mirror spacing or pore width of lobster eye optics," English, *Astronomische Nachrichten*, vol. 339, no. 5, SI, pp. 363–366, Jan. 2018.
11. R. Filgas, "Space radiation monitoring with timepix," English, *Astronomische Nachrichten*, vol. 339, no. 5, SI, pp. 386–390, Jan. 2018.
12. R. Hudec, "Low-dispersion spectroscopy with cubesats and photographic plates," English, *Astronomische Nachrichten*, vol. 339, no. 5, SI, pp. 416–419, Jan. 2018.
13. R. Hudec, "Axro introduction and historical background," English, *Contributions of the Astronomical Observatory Skalnate Pleso*, vol. 48, no. 3, pp. 396–404, 2018.
14. R. Hudec and K. Remisova, "Biomimetics and astronomical x-ray optics," English, *Contributions of the Astronomical Observatory Skalnate Pleso*, vol. 47, no. 2, pp. 67–75, 2017.
15. R. Hudec and S. Michalova, "Fish eye optics," English, *Contributions of the Astronomical Observatory Skalnate Pleso*, vol. 47, no. 2, pp. 94–99, 2017.
16. R. Hudec, "Astrophysical payloads for picosatellites," English, *Contributions of the Astronomical Observatory Skalnate Pleso*, vol. 47, no. 2, pp. 143–150, 2017.
17. I. Vertat, R. Linhart, J. Masopust, A. Vobornik, and L. Dudacek, "Earth's thermal radiation sensors for attitude determination systems of small satellites," English, *Contributions of the Astronomical Observatory Skalnate Pleso*, vol. 47, no. 2, pp. 157–164, 2017.
18. V. Simon, "Perspectives of the lobster-eye telescope: The promising types of cosmic x-ray sources," English, *Contributions of the Astronomical Observatory Skalnate Pleso*, vol. 47, no. 2, pp. 184–191, 2017.

V. Dániel, L. Pína, A. Inneman, V. Zadražil, T. Báča, M. Platkevič, *et al.*, "Terrestrial gamma-ray flashes monitor demonstrator on cubesat," vol. 9978, 2016, ISBN: 9781510603479

1. A. Alanazi and J. Straub, "Engineering methodology for student-driven cubesats," English, *Aerospace*, vol. 6, no. 5, Jan. 2019.
2. R. Hudec, "X/euv and uv optics for miniature cube satellites payloads," English, in *EUV and X-Ray Optics: Synergy Between Laboratory and Space VI*, vol. 11032, 1000 20TH ST, PO BOX 10, BELLINGHAM, WA 98227-0010 USA: SPIE-INT SOC OPTICAL ENGINEERING, 2019.
3. A. Alanazi, A. B. Jones, and J. Straub, "Requirements modeling language and automated testing for cubesats," English, in *2019 IEEE Autotestcon*, 345 E 47TH ST, NEW YORK, NY 10017 USA: IEEE, 2019.

4. P. Hatfield, W. Furnell, A. Shenoy, E. Fox, R. Parker, and L. Thomas, "The lucid-timepix spacecraft payload and the cern school educational programme," English, *Journal of Instrumentation*, vol. 13, Jan. 2018.
5. R. Hudec, "Axro introduction and historical background," English, *Contributions of the Astronomical Observatory Skalnate Pleso*, vol. 48, no. 3, pp. 396–404, 2018.
6. R. Hudec and K. Remisova, "Biomimetics and astronomical x-ray optics," English, *Contributions of the Astronomical Observatory Skalnate Pleso*, vol. 47, no. 2, pp. 67–75, 2017.
7. R. Hudec and S. Michalova, "Fish eye optics," English, *Contributions of the Astronomical Observatory Skalnate Pleso*, vol. 47, no. 2, pp. 94–99, 2017.
8. R. Hudec, "Astrophysical payloads for picosatellites," English, *Contributions of the Astronomical Observatory Skalnate Pleso*, vol. 47, no. 2, pp. 143–150, 2017.

M. Urban, **O. Nentvich**, V. Stehlikova, T. Baca, V. Daniel, and R. Hudec, "Vzlusat-1: Nanosatellite with miniature lobster eye x-ray telescope and qualification of the radiation shielding composite for space application," *Acta Astronautica*, vol. 140, pp. 96–104, Nov. 2017, ISSN: 0094-5765

1. V. V. Lider, "Grazing-incidence focusing optics for x-ray telescopes (review)," English, *Instruments and Experimental Techniques*, vol. 65, no. 2, pp. 191–217, Jan. 2022.
2. D. Panek, T. Orosz, P. Karban, D. C. D. Gnawa, and H. K. Neghab, "Performance comparison of quantized control synthesis methods of antenna arrays," English, *Electronics*, vol. 11, no. 7, Jan. 2022.
3. M. May, G. D. Rupakula, and P. Matura, "Non-polymer-matrix composite materials for space applications," English, *Composites Part C: Open Access*, vol. 3, Jan. 2020.
4. J. J. Lopez-Salamanca, L. O. Seman, M. D. Berejuck, and E. A. Bezerra, "Finite-state markov chains channel model for cubesats communication uplink," English, *IEEE Transactions on Aerospace and Electronic Systems*, vol. 56, no. 1, pp. 142–154, Jan. 2020.
5. R. Filgas, M. Malich, T. Kuwahara, *et al.*, "Risepix — a timepix-based radiation monitor telescope onboard the risesat satellite," English, *Astronomische Nachrichten*, vol. 340, no. 7, SI, pp. 674–680, Jan. 2019.
6. W. Furnell, A. Shenoy, E. Fox, and P. Hatfield, "First results from the lucid-timepix spacecraft payload onboard the techdemosat-1 satellite in low earth orbit," English, *Advances In Space Research*, vol. 63, no. 5, pp. 1523–1540, Jan. 2019.
7. P. Hatfield, W. Furnell, A. Shenoy, E. Fox, R. Parker, and L. Thomas, "The lucid-timepix spacecraft payload and the cern school educational programme," English, *Journal of Instrumentation*, vol. 13, Jan. 2018.

8. R. Filgas, "Space radiation monitoring with timepix," English, *Astronomische Nachrichten*, vol. 339, no. 5, SI, pp. 386–390, Jan. 2018.

V. Daniel, A. Inneman, L. Pina, V. Zadrazil, V. B. T., Stehlikova, *et al.*, "X-ray lobster eye all-sky monitor for rocket experiment," R. Hudec and L. Pina, Eds., Conference on EUV and X-ray Optics - Synergy between Laboratory and Space V, Prague, Czech Republic, APR 26-27, 2017, vol. 10235, Spie-int soc Optical Engineering, 2017, ISBN: 978-1-5106-0971-6; 978-1-5106-0972-3

1. M. Ouyang, X. Zhao, W. He, *et al.*, "Structural design method of the meridional lobster-eye lens with optimal efficiency," English, *Applied Optics*, vol. 58, no. 33, pp. 9033–9038, Jan. 2019.
2. R. Filgas, M. Malich, T. Kuwahara, *et al.*, "Risepix — a timepix-based radiation monitor telescope onboard the risesat satellite," English, *Astronomische Nachrichten*, vol. 340, no. 7, SI, pp. 674–680, Jan. 2019.
3. R. Filgas, "Space radiation monitoring with timepix," English, *Astronomische Nachrichten*, vol. 339, no. 5, SI, pp. 386–390, Jan. 2018.
4. R. Hudec, "Low-dispersion spectroscopy with cubesats and photographic plates," English, *Astronomische Nachrichten*, vol. 339, no. 5, SI, pp. 416–419, Jan. 2018.
5. R. Hudec, "Axro introduction and historical background," English, *Contributions of the Astronomical Observatory Skalnate Pleso*, vol. 48, no. 3, pp. 396–404, 2018.
6. R. Hudec, "Astrophysical payloads for picosatellites," English, *Contributions of the Astronomical Observatory Skalnate Pleso*, vol. 47, no. 2, pp. 143–150, 2017.

R. Hudec, L. Pina, V. Marsikova, **O. Nentvich**, A. U. M., and Inneman, "Kirkpatrick baez x-ray optics for astrophysics: Recent status," *Contributions Of The Astronomical Observatory Skalnate Pleso*, vol. 48, pp. 437–445, 3 2018, ISSN: 1335-1842

1. V. V. Lider, "Grazing-incidence focusing optics for x-ray telescopes (review)," English, *Instruments and Experimental Techniques*, vol. 65, no. 2, pp. 191–217, Jan. 2022.
2. S. Rukdee, V. Burwitz, G. Hartner, *et al.*, "X-ray ray tracing with zemax for the panter testing facility," English, in *Optics for EUV, X-Ray, and Gamma-ray Astronomy X*, vol. 11822, 1000 20TH ST, PO BOX 10, BELLINGHAM, WA 98227-0010 USA: SPIE-INT SOC OPTICAL ENGINEERING, 2021.
3. J. Shen, N. An, W. Zhang, X. Du, and Q. Wang, "Monochromatic kirkpatrick-baez microscope using two spherically bent crystals," English, in *International Conference on Optoelectronic and Microelectronic Technology and Application*, vol. 11617, 1000 20TH ST, PO BOX 10, BELLINGHAM, WA 98227-0010 USA: SPIE-INT SOC OPTICAL ENGINEERING, 2020.

4. V. V. Lider, "Kirkpatrick-baez and wolter x-ray focusing optics (review)," English, *Journal of Surface Investigation*, vol. 13, no. 4, pp. 670–682, Jan. 2019.
5. D. Longcope, L. Acton, and C. Kankelborg, "Practical, corrected kirkpatrick-baez telescope for x-ray astronomy," English, *Applied Optics*, vol. 58, no. 18, pp. 4969–4980, Jan. 2019.
6. V. Burwitz, R. Willingale, G. Pareschi, *et al.*, "Ahead joint research activity on x-ray optics," English, in *Space Telescopes and Instrumentation 2018: Ultraviolet To Gamma Ray*, vol. 10699, 1000 20TH ST, PO BOX 10, BELLINGHAM, WA 98227-0010 USA: SPIE-INT SOC OPTICAL ENGINEERING, 2018.

M. Urban, **O. Nentvich**, V. Stehlikova, and L. Sieger, "Uncooled spectrometer for x-ray astrophysics," R. Hudec and L. Pina, Eds., Conference on EUV and X-ray Optics - Synergy between Laboratory and Space V, Prague, Czech Republic, APR 26-27, 2017, vol. 10235, Spie-int soc Optical Engineering, 2017, ISBN: 978-1-5106-0971-6; 978-1-5106-0972-3

1. R. Hudec, "Axro introduction and historical background," English, *Contributions of the Astronomical Observatory Skalnate Pleso*, vol. 48, no. 3, pp. 396–404, 2018.
2. R. Hudec and K. Remisova, "Biomimetics and astronomical x-ray optics," English, *Contributions of the Astronomical Observatory Skalnate Pleso*, vol. 47, no. 2, pp. 67–75, 2017.
3. R. Hudec and S. Michalova, "Fish eye optics," English, *Contributions of the Astronomical Observatory Skalnate Pleso*, vol. 47, no. 2, pp. 94–99, 2017.
4. R. Hudec, "Astrophysical payloads for picosatellites," English, *Contributions of the Astronomical Observatory Skalnate Pleso*, vol. 47, no. 2, pp. 143–150, 2017.
5. R. Hudec and T. Doehring, "Jeumico: Czech-bavarian astronomical x-ray optics project," English, *Contributions of the Astronomical Observatory Skalnate Pleso*, vol. 47, no. 2, pp. 170–177, 2017.

V. Stehlikova, M. Urban, **O. Nentvich**, V. Daniel, L. Sieger, and J. Tutt, "Hard x-ray vela supernova observation on rocket experiment wrx-r," *Contributions Of The Astronomical Observatory Skalnate Pleso*, vol. 47, pp. 165–169, 2 2017, ISSN: 1335-1842

1. M. Ouyang, Y. Fu, J. Zhou, *et al.*, "Comprehensive understanding of the focal property of lobster-eye optics," English, *Applied Optics*, vol. 59, no. 14, pp. 4263–4270, Jan. 2020.
2. R. Hudec, L. Amati, F. Frontera, *et al.*, "Esa theseus and czech participation," English, *Astronomische Nachrichten*, vol. 341, no. 3, pp. 348–355, Jan. 2020.
3. T. Baca, D. Turecek, R. McEntaffer, and R. Filgas, "Rospix: Modular software tool for automated data acquisitions of timepix detectors on robot operating system," English, *Journal of Instrumentation*, vol. 13, Jan. 2018.

4. I. Vertat and P. Fiala, "Compensation of industrial cmos camera and image enhancement for sounding rocket astrophysical experiments," English, in *2018 23rd International Conference on Applied Electronics (AE)*, 345 E 47TH ST, NEW YORK, NY 10017 USA: IEEE, 2018, pp. 149–153.
5. R. Hudec, "Axro introduction and historical background," English, *Contributions of the Astronomical Observatory Skalnate Pleso*, vol. 48, no. 3, pp. 396–404, 2018.

V. Daniel, M. Urban, **O. Nentvich**, and V. Stehlikova, "Vzlusat-1: Verification of new materials and technologies for space," T. S. Pagano, Ed., Conference on CubeSats and NanoSats for Remote Sensing, San Diego, CA, AUG 31, 2016, vol. 9978, Spie-int soc Optical Engineering, 2016, ISBN: 978-1-5106-0347-9; 978-1-5106-0348-6

1. I. Vertat, R. Llnhart, M. Pokorny, J. Masopust, P. Fiala, and J. Mraz, "Small satellite ground station in pilsen - experiences with vzlusat-1 commanding and future modifications toward open reference ground station solution," English, in *2018 28th International Conference Radioelektronika (Radioelektronika)*, 345 E 47TH ST, NEW YORK, NY 10017 USA: IEEE, 2018.
2. R. Hudec, "Axro introduction and historical background," English, *Contributions of the Astronomical Observatory Skalnate Pleso*, vol. 48, no. 3, pp. 396–404, 2018.
3. I. Vertat, R. Linhart, L. Dudacek, V. Daniel, and P. Svoboda, "Autonomous and semi-autonomous radio commanding of vzlusat-1 nanosatellite from ground control station in pilsen," English, in *2017 International Conference on Applied Electronics (AE)*, 345 E 47TH ST, NEW YORK, NY 10017 USA: IEEE, 2017, pp. 263–268.
4. R. Hudec, "Astrophysical payloads for picosatellites," English, *Contributions of the Astronomical Observatory Skalnate Pleso*, vol. 47, no. 2, pp. 143–150, 2017.

V. Stehlikova, M. Urban, **O. Nentvich**, A. Inneman, T. Doehring, and A.-C. Probst, "Study of lobster eye optics with iridium coated x-ray mirrors for a rocket experiment," R. Hudec and L. Pina, Eds., Conference on EUV and X-ray Optics - Synergy between Laboratory and Space V, Prague, Czech Republic, APR 26-27, 2017, vol. 10235, Spie-int soc Optical Engineering, 2017, ISBN: 978-1-5106-0971-6; 978-1-5106-0972-3

1. T. Baca, M. Jilek, P. Manek, *et al.*, "Timepix radiation detector for autonomous radiation localization and mapping by micro unmanned vehicles," English, in *2019 IEEE/RSJ International Conference on Intelligent Robots and Systems (IROS)*, 345 E 47TH ST, NEW YORK, NY 10017 USA: IEEE, 2019, pp. 1129–1136.

2. M. Holynska, A. Tighe, and C. Semprimoschnig, "Coatings and thin films for spacecraft thermo-optical and related functional applications," English, *Advanced Materials Interfaces*, vol. 5, no. 11, Jan. 2018.
3. I. Vertat and P. Fiala, "Compensation of industrial cmos camera and image enhancement for sounding rocket astrophysical experiments," English, in *2018 23rd International Conference on Applied Electronics (AE)*, 345 E 47TH ST, NEW YORK, NY 10017 USA: IEEE, 2018, pp. 149–153.
4. R. Hudec, "Axro introduction and historical background," English, *Contributions of the Astronomical Observatory Skalnate Pleso*, vol. 48, no. 3, pp. 396–404, 2018.

V. Daniel, A. Inneman, I. Vertat, T. Baca, M. N. O., Urban, *et al.*, "In-orbit commissioning of czech nanosatellite vzlusat-1 for the qb50 mission with a demonstrator of a miniaturised lobster-eye x-ray telescope and radiation shielding composite materials," *Space Science Reviews*, vol. 215, 5 Aug. 2019, ISSN: 0038-6308

1. J. Chen, L. Liu, W. Xu, X. Huang, and H. Sheng, "Design and analysis of a hollow metallic microlattice active cooling system for microsatellites," English, *Nanomaterials*, vol. 12, no. 9, Jan. 2022.
2. E. Banken, V. E. Schneider, M. K. Ben-Larbi, L. Pambaguian, and J. Oeffner, "Biomimetic space debris removal: Conceptual design of bio-inspired active debris removal scenarios," English, *Ceas Space Journal*, vol. 15, no. 1, SI, pp. 237–252, Jan. 2023.
3. M. M. Hassan and G. M. Rather, "Innovative relay selection and optimize power allocation for free space optical communication," English, *Optical and Quantum Electronics*, vol. 53, no. 12, Jan. 2021.
4. A. Kear and S. L. Folkes, "A solution to the hyper complex, cross domain reality of artificial intelligence: The hierarchy of ai," English, *International Journal of Advanced Computer Science and Applications*, vol. 11, no. 3, pp. 49–59, Jan. 2020.

T. Baca, M. Jilek, I. Vertat, M. Urban, **O. Nentvich**, R. Filgas, *et al.*, "Timepix in leo orbit onboard the vzlusat-1 nanosatellite: 1-year of space radiation dosimetry measurements," *Journal of Instrumentation*, vol. 13, Nov. 2018, 20th International Workshop on Radiation Imaging Detectors, Sundsvall, Sweden, JUN 24-28, 2018, ISSN: 1748-0221

1. R. Hudec, "X/euv and uv optics for miniature cube satellites payloads," English, in *EUV and X-Ray Optics: Synergy Between Laboratory and Space VI*, vol. 11032, 1000 20TH ST, PO BOX 10, BELLINGHAM, WA 98227-0010 USA: SPIE-INT SOC OPTICAL ENGINEERING, 2019.

R. Hudec, L. Pina, V. Marsikova, **O. Nentvich**, A. U. M., and Inneman, "Lobster eye x-ray optics for astrophysics: Recent status," *Contributions Of The Astronomical Observatory Skalnate Pleso*, vol. 48, pp. 456–465, 3 2018, ISSN: 1335-1842

1. V. V. Lider, "Grazing-incidence focusing optics for x-ray telescopes (review)," English, *Instruments and Experimental Techniques*, vol. 65, no. 2, pp. 191–217, Jan. 2022.

L. Mikulickova, L. Pina, A. Inneman, D. Doubravova, V. Marsikova, L. Sieger, *et al.*, "Optimization of microroughness of replicated x-ray optics," R. Hudec and L. Pina, Eds., Conference on EUV and X-ray Optics - Synergy between Laboratory and Space V, Prague, Czech Republic, APR 26-27, 2017, vol. 10235, Spie-int soc Optical Engineering, 2017, ISBN: 978-1-5106-0971-6; 978-1-5106-0972-3

1. M. Holynska, A. Tighe, and C. Semprimoschnig, "Coatings and thin films for spacecraft thermo-optical and related functional applications," English, *Advanced Materials Interfaces*, vol. 5, no. 11, Jan. 2018.

L. Pina, R. Hudec, A. Inneman, **O. Nentvich**, V. U. M., Marsikova, *et al.*, "Multi-foil x-ray optics tests at panter: Preliminary results," *Contributions Of The Astronomical Observatory Skalnate Pleso*, vol. 48, pp. 466–475, 3 2018, ISSN: 1335-1842

1. M. Ouyang, Y. Fu, J. Zhou, *et al.*, "Comprehensive understanding of the focal property of lobster-eye optics," English, *Applied Optics*, vol. 59, no. 14, pp. 4263–4270, Jan. 2020.

V. Stehlikova, M. Urban, **O. Nentvich**, and L. Sieger, "Radiation resistance monitor on vzlusat-1: Preliminary results," *Astronomische Nachrichten*, vol. 339, pp. 382–385, 5, SI Jun. 2018, ISSN: 0004-6337

1. T. Blachowicz and A. Ehrmann, "Shielding of cosmic radiation by fibrous materials," English, *Fibers*, vol. 9, no. 10, Jan. 2021.

M. Urban, **O. Nentvich**, T. Baca, I. Vertat, V. Marsikova, D. Doubravova, *et al.*, "Rex: X-ray experiment on the water recovery rocket," *Acta Astronautica*, vol. 184, pp. 1–10, Jul. 2021, ISSN: 0094-5765

1. V. Simon and R. Hudec, "Perspectives of the lobster-eye monitor in the soft x-ray observing the galactic center region," English, *Journal of High Energy Astrophysics*, vol. 35, pp. 69–76, Jan. 2022.

V. Daniel, R. Hudec, T. Baca, L. Pina, A. Inneman, V. Marsikova, *et al.*, "Rex le x-ray telescope experiment overview," R. Hudec and L. Pina, Eds., Conference on EUV and X-Ray Optics - Synergy between Laboratory and Space VI, Prague, Czech Republic, APR 03-04, 2019, vol. 11032, Spie-int soc Optical Engineering, 2019, ISBN: 978-1-5106-2731-4

1. V. Daniel, P. Svoboda, M. Junas, *et al.*, "Development of cubesat with cots camera enabling eo with high gsd," English, in *Sensors, Systems, and Next-generation Satellites XXIv*, vol. 11530, 1000 20TH ST, PO BOX 10, BELLINGHAM, WA 98227-0010 USA: SPIE-INT SOC OPTICAL ENGINEERING, 2020.